Petrogenetic and economic significance of the whole-rock chemistry of ultramafic cumulates in the Cape Smith foldbelt, northern Quebec

David Clark
Dept. of Earth & Planetary Sciences
McGill University, Montreal

A thesis submitted to McGill University in partial fulfillment of the requirements of the degree of Master of Science

May 2008

Your file Votre référence
ISBN: 978-0-494-51080-3
Our file Notre référence
ISBN: 978-0-494-51080-3

Abstract

The ultramafic cumulate rocks of the Raglan horizon in the Proterozoic Cape Smith fold belt of northern Quebec have a common parental liquid in equilibrium with olivine of Fo_{89} composition. Cumulate olivines have experienced a trapped liquid shift to lower forsterite composition proportionally to the fraction of trapped liquid in the cumulate. Anomalously low nickel contents in analyses of both olivine and whole-rock chemistries are observed only in cumulates with the most modal olivine and which are proximal to known Ni-Cu-(PGE) deposits. The calculated compositions of the trapped liquid fraction indicate that most of the Raglan cumulates formed from Fe-rich high-MgO basalts, which are restricted to the base of the Chukotat volcanic stratigraphy. We propose that a lower degree of adiabatic partial melting of a mantle source accounts for the Fe-rich nature of these parental liquids and may provide an explanation for the presence of numerous Ni-Cu-(PGE) deposits in the sills of the Raglan horizon.

Résumé

Les cumulats ultramafiques de l'horizon de Raglan, situé dans la ceinture plissée de Cape Smith dans le Nord du Québec, ont un liquide parent commun qui est en équilibre avec l'olivine de composition Fo_{89}. La composition des olivines cumulus a été modifiée à cause de la présence d'un liquide piégé. Leur composition a changé vers une composition moins forstéritique, et le changement a été proportionnel à la fraction de liquide piégé dans le cumulat. Des teneurs en nickel anomalement basses à la fois dans l'olivine et dans la roche sont observées uniquement dans les cumulats qui contiennent la plus grande proportion d'olivine modale et qui se situent proche des gîtes connus de Ni-Cu-(EGP). Les compositions calculées de la fraction de liquide pig indiquent que la plupart des cumulats de Raglan se sont formés à partir de basaltes à haute teneur en MgO et riches en Fe, lesquels sont restreints à la base de la séquence volcanique de Chukotat. Nous proposons qu'un taux de fusion partielle adiabatique relativement bas d'une source mantellique soit la cause de la composition riche en fer de ces liquides parents ; ce mécanisme peut expliquer la présence de gîtes nombreux de Ni-Cu-(EGP) dans les filons-couches de l'horizon de Raglan.

Contents

1 Contributions of authors

The manuscript included in this thesis is authored by David Clark and Don Francis. The original impetus for the thesis was provided by Phil Vicker (Falconbridge Ltd.) and Don Francis (McGill University), who conceived of the original diamond drill hole (DDH) sampling program. The Falconbridge Ltd. DDH database was queried by David Clark, and appropriate DDH cores were located and sampled by the same at the Donaldson exploration camp core-farm. Whole-rock analyses were performed by SGS Lakefield, Lakefield ON. Microprobe analyses were performed by David Clark, with the assistance of Glenn Poirier at McGill University. Logistical and financial support was provided by Falconbridge Ltd. Additional financial support was provided by an NSERC operating grant to Don Francis and by the Department of Earth & Planetary Science, McGill University. Data analysis, and manuscript and figure composition is by David Clark with the frequent input and guidance of Don Francis. An early draft of this manuscript was reviewed by Tom Clark (Géologie Québec), and the final version was reviewed by Don Francis.

2 Introduction

Interpreting the chemistry of cumulate sills or flows is problematic because of the non-unique nature of processes that lead to their formation. Because the composition of magma in a sill conduit system can be modified by several processes, including crystal fractionation, sill compaction, effects of assimilation, trapped liquid re-equilibration, and metamorphism, it can be difficult to regard cumulate compositions as useful in investigations into petrogenesis of the associated magmatic systems. Consequently, relatively little attention has been paid to the chemistry of such sills. Ultramafic cumulate sills are the frequent hosts of Ni-Cu-(PGE) magmatic sulphide deposits, such as those found in the Cape Smith foldbelt, and if any insight can be obtained from the study of their compositions, it may help advance our understanding of the parental magma compositions and physical conditions necessary for the formation of these deposits.

The research project that is the focus of this thesis was instigated by Phil Vicker of Falconbridge Limited and Don Francis of the Dept. of Earth & Planetary Sciences, McGill University. They observed that rare ultramafic cumulates in the Raglan horizon retained their primary mineralogy and wondered what insights might be gleaned from a systematic study of the fresh cumulate rocks from across the Falconbridge Raglan property. The Raglan horizon ultramafics have been the subject of considerable study by Falconbridge Ltd. in the context of mineral exploration, but these studies have only considered the far more common greenschist facies metamorphosed ultramafic rocks, whose primary mineralogy has been completely replaced by serpentine and talc alteration, and whose volatile contents can reach up to

20 weight percent. The author has spent six summers in the Cape Smith foldbelt in the context of both academic and mineral exploration work, and has only very rarely encountered ultramafic rocks containing primary olivine. Fresh cumulates are different enough in appearance from their serpentinized equivalents that Falconbridge drill-core loggers frequently mis-identified fresh intervals in drill core logs, completely missing the presence of fresh olivine. Despite a very extensive database of diamond drill hole (DDH) logs spanning several decades, identifying ultramafic units containing unaltered intervals is less than trivial. However, drill core loggers at Falconbridge systematically sent unidentified, problematic, and representative core samples for major-element whole-rock analysis. Thus, a significant proprietary Falconbridge database of whole-rock chemistry exists for the Raglan horizon. The vast majority of the ultramafic rock samples in this database are altered, but samples with coinciding low loss-on-ignition (LOI) and high MgO contents were found to often contain fresh olvine, although the presence of this olivine was rarely noted in DDH logs. The author identified five intervals of drill core in the Falconbridge database based on this criterion, and comprehensively sampled their fresh portions.

The whole-rock and olivine compositions that were determined for this thesis reveal that a variety of information is in fact contained in the sills of the Raglan horizon. This includes insights into the processes responsible for the economic accumulations of magmatic sulphide Ni-Cu-(PGE) deposits, as well as the nature of the sill parental liquids. These findings advance our understanding of the petrogenesis of the Raglan horizon and associated Ni-Cu-(PGE) deposits.

3 Manuscript to be submitted to Lithos

Petrogenetic and economic significance of the whole-rock chemistry of ultramafic cumulates in the Cape Smith foldbelt, northern Quebec

David Clark & Don Francis

Department of Earth & Planetary Sciences, McGill University,

3450 University St., Montreal, Quebec, Canada, H3A 2A7

Preprint submitted to Lithos *2 May 2008*

Abstract

The Cape Smith foldbelt is a Proterozoic fold and thrust belt located in northern Quebec, whose Raglan horizon is host to ultramafic cumulate sills containing important magmatic-sulphide Ni-Cu-(PGE) deposits. In this study, five unaltered sills from mineralized and unmineralized environments across 40 km of the Raglan horizon were sampled. The ultramafic cumulate rocks span both a range of modal olivine concentrations and forsterite contents, the latter reflecting the effect of a post-emplacement trapped liquid shift proportional to the amount of trapped liquid present; calculated magmatic olivine compositions have forsterite contents of Fo_{89}. The calculated parental liquid in equilibrium withs have compositions equivalent to the volumetrically-rare Fe-enriched picrites found at the base of the overlying Chukotat volcanic pile, and are interpreted as representing a lower degree of mantle partial melting than that which led to the formation of most of the Chukotat basalt sequence. Samples associated with unmineralized environments are high tenor (13.5% Ni) while those associated with mineralized environments are low-tenor (7.5% Ni); this is equivalent to an R-factor 2 to 3 times lower in the mineralized environment. Assimilation of sulphur-rich sediments is likely responsible for the lowered R-factor in the samples from mineralized environments. The parental Fe-rich magmas have characteristics favourable to assimilation of sediments: they are the first magmas erupted in the Chukotat volcanic sequence and are at higher temperatures than subsequent Chukotat magmas, both increasing the likelyhood of interaction with sulphur-bearing sediments.

Email addresses: dclark@eps.mcgill.ca (David Clark), donf@eps.mcgill.ca (Don Francis).

List of Tables

List of Figures

1 Introduction

The bulk chemistry and mineralogy of cumulate magmatic rocks is controlled by a large number of parameters and processes. These include the composition of the parent magma, crystal fractionation, magma mixing, the fraction of crystals in the cumulate, filter pressing, assimilation, trapped liquid crystallization and re-equilibration, and metamorphism. The bulk chemistry of cumulate rocks has received relatively little attention because the processes leading to their formation are non-unique. However, in simple magmatic systems, such as conduit systems of ultramafic sills and dykes, fewer processes are operative, and valuable information may be recorded in the bulk compositions of cumulate rocks.

The Raglan horizon of the Cape Smith foldbelt hosts a series of ultramafic cumulate sillls which contain numerous Ni-Cu-(PGE) deposits. Typically, these sills are pervasively serpentinized (volatile contents often greater than 20 wt%). The serpentinization process causes movement of the more mobile chemical species and overprints the magmatic history recorded in the cumulate rock compositions. Rare units within the Raglan horizon are unserpentinized and our results show that the bulk chemistry of these units yields insights into both petrogenesis and ore formation processes operation during the formation of the sills.

Our results show that the overlying Chukotat basalt sequences, though associated with the sill systems, cannot be taken as direct proxies for the parental liquids that ran through the sill conduit systems. Rather, possible parental liquids are restricted to volumetrically rare Fe-enriched high-MgO picrites found

only in the lowermost Chukotat sequence. It is significant that the Raglan horizon sills appear to be genetically linked only to the lowermost, compositionally distinct Fe-enriched Chukotat basalts because the Raglan horizon is significantly mineralized while other cumulate sills horizons in the foldbelt are not. While there are likely a multiplicity of factors leading to the ultimate formation of these ore deposits, a distinct magma type having characteristics favourable to ore-deposition is likely an important one. We show that the formation of Ni-Cu-(PGE) deposits is documented in whole-rock chemistry at specific levels within sill stratigraphy and that those samples showing evidence for the loss of significant nickel to deposit formation processes also have different tenors than samples that do not show this evidence. Given that the nickel concentrations in the parental liquids are not likely to change significantly through normal fractionation processes in the sill system, it is likely that a process, such as sulphur-rich sediment assimilation, has changed magma system R-factors and lowered tenors during ore-formation processes.

2 Geological setting

The Cape Smith belt is an early-Proterozoic volcano-sedimentary fold and thrust belt in northern Quebec, Canada. It records the rifting and development of an oceanic basin (e.g. Hynes and Francis, 1982; Francis et al., 1983; Picard et al., 1990), and subsequent convergence-related deformation (e.g. St-Onge et al., 1992). Two major fault-bounded groups are associated with rifting and oceanic-plate creation: the Povungnituk (also: Purvirnituq) and Chukotat groups, respectively. The base of the Povungnituk Group, has been dated at 2038 Ma (Machado et al., 1990), while a rhyolite in the upper part

has yielded an age of 1959 Ma (Parrish, 1989). The group is comprised of intercalated rift-related metasediments and subaqueous tholeiites with an OIB chemical signature (Francis et al., 1983; Modeland et al., 2003). The structurally overlying Chukotat Group, whose inferred maximum age is 1918 Ma (Parrish, 1989), consists of fault-bounded repetitive sequences of subaqueous picritic to tholeiitic basalts (Francis et al., 1981). The basalts of the Chukotat Group have trace-element patterns similar to those of modern mid-ocean ridge basalts (MORB), and the high-MgO olivine-phyric members could represent primary liquids in equilibrium with Earth's upper mantle (Francis et al., 1983).

Metamorphic grades in the Povungnituk and Chukotat groups range from lower greenschist to middle amphibolite, and are thought to result from an arc–continent collision causing in-sequence and out-of-sequence thrusting and imbrication of Proterozoic cover units (Bégin, 1989). In accordance with local convention and clarity of argument, the rocks are referred to by their protolith names e.g. pyroxenite for amphibolite, peridotite for serpentinite, etc.

Povungnituk Group rocks are intruded by massive gabbroic sills that have been interpreted as feeder systems for Povungnituk Group volcanics (St-Onge and Lucas, 1993). Both the Povungnituk and Chukotat groups are intruded by thin mafic–ultramafic and ultramafic sills, interpreted as feeder systems for the Chukotat basalts (Bédard et al., 1984). Sills at the base of the Chukotat Group comprise the Raglan horizon and host economic Ni-Cu-(PGE) magmatic-sulphide deposits (e.g. Giovenazzo et al., 1989).

Typical mafic-ultramafic sills of the Raglan horizon comprise a pyroxenitic lower unit of variable thickness (generally between 1 and 10 m), which grades

upwards to pyroxenitic peridotite or peridotite. The peridotite is most commonly completely serpentinized, homogeneous, and massive, although it is frequently cut by serpentine and magnetite veins. Magmatic and remobilized Ni-Cu-(PGE) sulphide deposits occur as pods at the base of the ultramafic sills, commonly in magmatic or structural embayments. The upper parts of the sills are pyroxenitic to gabbroic; the pyroxenite examples are similar in composition, thickness, and texture to the pyroxenite margins. Well-developed metre-scale hexagonal columnar jointing is commonly observed in the ultramafic rocks. Many sills are folded and/or boudinaged, although encasing sediments often take up much of the deformation. The ultramafic sills of the Raglan horizon at the base of the Chukotat Group are generally interpreted as cumulates formed by the accumulation of olivine crystals in the magma conduits of early Chukotat olivine-phyric basaltic volcanism.

3 Sampling and petrography

This study focuses on almost unmetamorphosed sections of the ultramafic sills of the Raglan horizon, which underlies the Chukotat Group volcanics (Fig. 1). Core samples from peridotites and pyroxenites containing fresh primary olivine were identified in a Falconbridge Ltd. whole-rock chemistry database for the Raglan property on the basis of low loss-on-ignition (LOI) and high MgO content. Once identified, cores were sampled from the unaltered portions of five different ultramafic sills which are referred to here as sections A through E. Four of these are located in the main Raglan horizon (A, B, C, D), two being proximal to the major Katinniq Ni-Cu-(PGE) deposit (A, B). The remaining sill (E) is located higher in the stratigraphy and its relationship to the Raglan

horizon is unclear. Our sections are spread over a strike distance of 40 km along the base of the Chukotat Group (Fig. 1).

Olivine, chrome spinel, clinopyroxene, and sulphides are the primary minerals in the sampled ultramafic rocks. Olivine and chrome spinel are cumulus, while clinopyroxene and sulphides are intercumulus. Samples are medium grained and exhibit no preferred mineral orientation. The adcumulate samples contain up to 90% anhedral interlocking olivines forming a mosaic texture. The orthocumulates contain $\sim$ 50% olivines enclosed in a matrix composed mainly of interstitial clinopyroxene and its alteration products. Some of the olivines are also partially altered, with a marginal envelope of finely bladed serpentine oriented perpendicular to the grain boundaries. Chrome spinel is present both as inclusions in the olivine and disseminated in the matrix. Sulphides, where present, are disseminated and interstitial to the olivine. A representative SEM image of a typical unaltered peridotite is given in Fig. 2.

4 Rock and mineral chemistry

Whole-rock samples from the drill cores were analysed for major and selected trace elements by X-ray fluorescence spectrometry at SGS Lakefield, Lakefield ON, and olivine compositions were determined by electron microprobe at McGill University (Table 1). The olivines are compositionally unzoned and show no significant major-element variation within individual thin sections. Olivine forsterite content for all sills ranges from $Fo_{82.5}$ to Fo_{88} and correlates positively with both modal and normative total olivine. The compositions of chrome spinels, present as small euhedral crystals in the matrix or embedded in olivine, were measured by electron microprobe and used to determine an

oxidation state of $X_{Fe^{3+}} = 0.08$ (range 0.04–0.12, $\sigma = 0.02$) for the parental liquids, based on the calibration of Maurel & Maurel (1982).

The whole-rock and olivine data for sections A–E plotted against drill hole depth are given in Fig. 3 and are described as follows:

Section A (Fig. 3a) is for samples from the basal portion of a thick ultramafic sill located ~350 m down-dip of the nearest Katinniq ore lenses (G. Desharnais, Xstrata plc., personal communication, 2007). Both whole-rock and olivine $Mg^{\#}$ are fairly constant at Mg/(Mg + Fe) = 87 – 87.5 from ~600–780 m; however, they drop sharply as the MgO content of the rock decreases towards its lower margin. Whole-rock silicate nickel contents, determined by extrapolating whole-rock Ni to 0% S (Fig. 5), follow olivine Ni contents, and can be used as proxies for these in their absence. Over the interval of constant $Mg^{\#}$, olivine and silicate nickel contents are ~2000 ppm, but are anomalously low (~1000 ppm) in one sample in the ~670–690 m interval. Nickel contents are also anomalously low from 780–800 m as the sill's margin is approached. The marginal pyroxenites (810–820 m) have whole-rock silicate nickel contents that are indistinguishable from those of the uphole samples with constant $Mg^{\#}$, despite their higher total nickel contents (up to 1 wt% Ni).

Section B (Fig. 3b) is for samples from the middle portion of the same sill as section A, but is located 300 m to the East along strike. Forsterite contents of olivine are essentially the same as those in Section A. Olivine nickel contents at 900–1000 m are anomalously low, however, when compared to the Ni contents of samples from Section A. Over the interval for which olivine analyses are not available (700–900 m) the calculated whole-rock silicate nickel contents are similarly low. Apart from the samples with anomalous

nickel contents, both sections A and B record a monotonic decrease in nickel upwards at constant $Mg^{\#}$.

Section C (Fig. 3c) is located ~8.5 km along strike to the East of the Katinniq deposit (zone 13–14) and is for samples from an interval that is fairly constant in both $Mg^{\#}$ and Ni content and contains the most primitive olivine ($\sim Fo_{88}$) measured in this study. There are no known sulphide deposits in proximity to this section (G. Desharnais, Xstrata plc., personal communication, 2007). The variability in the whole-rock nickel contents reflects variable sulphur content, but the olivine nickel and calculated whole-rock silicate nickel values exhibit a monotonic decrease upwards, as in the case of sections A and B.

Section D (Fig. 3d) is for samples from the middle of a thin, barren sill 21 km along strike to the WSW of the Katinniq deposit. In contrast to the previous sections, whole-rock and olivine Ni concentrations increase up section with one jog to lower $Mg^{\#}$ and Ni at ~60 m, and bulk rock Ni content is lower than that of its contained olivine.

Section E contains the most MgO poor samples in this study with $Mg^{\#}$ 82–83, Ni = 2000 ppm. This section is not shown in Fig. 3 because the data were collected from a smaller interval than the other drill holes, and few olivine analyses could be obtained because of alteration.

The olivine nickel contents from all drill sections define two distinct trends in a diagram of Ni versus olivine Fo (Fig. 4). The shallower trend, which contains samples from all sections, is well-fit by an olivine equilibrium crystallization model involving an olivine-phyric Chukotat parental liquid (containing 300–500 ppm Ni; Francis et al., 1983). The steeper trend contains samples only from sections A and B, located near the Katinniq deposits and cannot be related to

the Chukotat parental liquid through the fractionation of any ferromagnesian mineral. These are the samples that exhibit relatively low Ni contents for a given $Mg^{\#}$ in sections A and B (Fig. 3a,b).

The nickel content of the bulk rock cumulates is controlled by the concentrations of nickel in olivine and in the sulphide phases, and their relative proportions as seen in a diagram of Ni versus S (Fig. 5). The whole-rock sample population with $> 0.1\%$ S define two trends: the steeper trend extrapolates to a massive (39% S) ore tenor of $\sim$13.5% Ni and a silicate (0% S) Ni content of $\sim$2000 ppm, while the shallower trend extrapolates to a massive ore tenor of $\sim$7.5% Ni and a silicate Ni content of $\sim$1300 ppm. All samples with $> 1.0\%$ S along the lower trend are from sections A and B, near the Katinniq deposit. Samples from section C lie along the higher tenor trend but generally contain $< 0.5\%$ S. Samples from sections D and E contain very little S but span a range of silicate Ni from 600–1700 ppm.

5 Discussion

5.1 Olivine sorting

The Raglan sills sampled in this study define a tight linear array between olivine and olivine-phyric Chukotat basalt in a cation diagram of (Mg + Fe) versus Si (Fig. 6). This suggests that olivine is the only major phase on the liquidus in the Raglan sills, despite the wide range of cumulate compositions, and that the Raglan cumulates represent variable amounts of binary mixing between olivine and olivine-phyric Chukotat basalt. The array in Fig. 6 lies slightly to the Si-poor side of a tie-line drawn between olivine and the olivine-

phyric Chukotat basalt, but is consistent with the presence of between 0.9 and 1.2 wt% cumulate chrome spinel (Si = 0, Mg + Fe = 33.33), enough to pull the entire array slightly off the olivine–Chukotat basalt mixing line.

The whole-rock data fall along an array with a slope that matches that predicted for olivine sorting in a Pearce element-ratio diagram (Pearce, 1968) constructed using Ti as a conserved element (Fig. 7). Furthermore, the fact that all the data from the sills define a single array with a common intercept indicates that the data are consistent with a single parental magma composition, despite the fact that samples come from different sills and are spread over 40 km of strike distance.

5.2 Primary olivine & parental liquids

If the bulk chemistry of the Raglan cumulate rocks involves only binary mixing between olivine and Chukotat parental liquid, then they should lie on tie-lines joining the olivines they contain to the olivine-phyric Chukotat basalts (Fig. 8). The measured olivine compositions range from Fo_{88} to Fo_{82} and are clearly too fayalite-rich to produce the observed cumulates from Chukotat olivine-phyric basalt. A tie-line between the most magnesian Chukotat basalt and the most magnesian cumulates, however, intersects the stoichiometric olivine line at Fo_{89}. This is even more convincingly demonstrated in a cation plot of $Mg^{\#}$ versus Si (Fig. 9), in which all olivine compositions must plot as a vertical array at Si = 33.3. Regressing the whole-rock sill data to this line gives the $Mg^{\#}$ ($\sim Fo_{89}$) of the whole-rock at 100% olivine. Furthermore, the most primitive Chukotat basalts would be in equilibrium with an olivine of Fo_{89}, determined using either the olivine–liquid Fe–Mg K_D of Roeder and Em-

slie (1970) or the MELTS thermodynamic software (Ghiorso and Sack, 1995). The most magnesian olivine reported to date in the Cape Smith foldbelt is $Fo_{88.5}$ (Stewart, 2002), measured in a dunite core sample from a sill in the the East Lake area ~10 km West of the Katinniq deposit.

The apparent contradiction between olivine sorting as the process responsible for chemical variability in the cumulates and the observation that the compositions of measured olivines do not fall on a mixing line in Mg–Fe space (Fig. 8) is resolved by considering the effect of continued crystallization of olivine in the postcumulus assemblage of olivine and trapped liquid. First investigated theoretically by Barnes (1986), the effect of this process has been observed in several suites of natural cumulates (e.g. Cawthorn et al., 1992; Lundgaard et al., 2006) and has been termed the *trapped liquid shift*. The additional crystallization and subsequent homogenization of cumulus phases in the postcumulus assemblage leads to more evolved cumulate-phase compositions than were originally in equilibrium with parental magmas. The magnitude of the shift is primarily a function of the proportion of trapped liquid in the cumulate. For example, Barnes (1986) showed that the olivines in an olivine cumulate with 10 wt% trapped liquid will experience a shift of 2 mol% to lower Fo; at 50 wt% trapped liquid the shift is 6 mol% Fo. Accordingly, we expect that those cumulates containing the greatest olivine content will have experienced the smallest shifts, and vice versa. The samples presented in this study span a range of normative olivine contents from 50% (section E) to 85% (section B), and correlate positively with measured olivine Fo contents (Fig. 8).

The peridotite cumulates in the dataset require a primary olivine of about Fo_{89} to be compatible with Chukotat basalt parent liquids, as argued previously. Assuming this to be the primary olivine composition, the Fe/Mg ratio of the

liquid in equilibrium with the olivine can be calculated using the olivine–liquid K_D (Roeder and Emslie, 1970). Given that the cumulate's final composition is a result of binary mixing of olivine and liquid, the three must be colinear in Fe–Mg space. The intersection of the Fe/Mg liquid equilibrium line and the line projected from Fo_{89} through the cumulate gives the liquid Fe and Mg composition, with the fractions of trapped liquid (X_l) and cumulate olivine (X_c) determined by the lever rule (Fig. 8). The remaining mafic components in the trapped liquid are then allowed to crystallized olivine and pyroxene in a 1:1 ratio after which the trapped-liquid olivine is averaged with the cumulate olivine to give the final olivine composition. This method yields final calculated olivine compositions that reproduce the observed olivine data closely, with ~80% of the olivines within 0.3 Fo units of the observed compositions.

5.3 Nickel-depletion signatures

The depletion of nickel observed in olivines associated with Ni-Cu-(PGE) magmatic-sulphide deposits has been discussed by several authors (e.g. Naldrett et al., 1984; Maier et al., 1998), and been proposed as an exploration tool (Maier et al., 1998). Anomalously low nickel concentrations at a given Fo content is interpreted to indicate that an immiscible sulphide liquid has segregated from the silicate liquid, extracting much of the nickel. The resultant silicate liquid and its equilbrium olivine are said to be nickel-depleted. The samples that plot on the steeper trend in Fig. 4, all from sections A and B, exhibit this nickel-depletion signature. In a Ni versus S diagram (Fig. 5), the whole-rock compositions of samples containing the nickel-depleted olivines lie on the shallow, 7.5% Ni tenor mixing line. Tenors observed in the massive

sulphide portions of the Katinniq deposits are generally in the range 7–9% Ni and thus we interpret the nickel depleted samples of sections A and B to record the sulphide segregation that led to the creation of the Katinniq deposits. Multiple massive sulphide lenses exist up-dip of sections A and B on the main footwall and ~150 m above the footwall (G. Desharnais, Xstrata plc., personal communication, 2007), stratigraphically equivalent to ~820 m and ~670 m depth in section A (Fig. 3a). The anomalously low Ni observed in section A at those depths may be compositional markers of the formation of the up-dip deposits.

The silicate–sulphide magma ratio (R-factor) is an often used tool in the study of magmatic suphide ore deposits (Campbell and Naldrett, 1979), as it relates parental magma metal content with ore tenor. Nickel tenor in our samples is high or low depending on whether the olivines record a loss of nickel to a sulphide phase. In the stratigraphy of sections A and B, both associated with proximal ore deposits, samples with both high and low nickel tenor are found. We suggest that the high tenor ores reflect the R-factor of a magma system not saturated with respect to sulphide until late in its depositional history i.e. one not actively exsolving and segregating a sulphide liquid as it passes through a conduit system. Late saturation of a sulphides is expected to generate small volumes of high-tenor ore (high R-factor). Where local sulphur-rich sediment assimilation by the picritic magmas has allowed a sulphide liquid to saturate and accumulate early enough to produce deposits, it is reasonable to expect that this extra sulphur source will be reflected by higher sulphide volumes and lower tenors (lower R-factor). Both the olivine and whole-rock chemistries are consistent with this idea: olivines that record a drastic loss in the nickel content of the silicate magma from which they were crystallizing are

in samples whose whole-rock compositions fall on the low-tenor mixing line. The remaining samples, both in sections A and B from which the samples with nickel-depleted olivines are from, as well as from the remaining sills, none of which are associated with Ni-Cu-(PGE) deposits, are all high-tenor.

The difference in R-factor necessary to account for the change from a 13.5% Ni tenor to a 7.5% Ni tenor can be calculated, assuming reasonable values for the partition coefficient of Ni between sulphide and silicate liquids (D_{Ni}), and silicate magma Ni contents. We take the former to be in the range 500–5000, experimentally determined for a komatiite–sulphide system at a range of f_{O_2} and f_{S_2} (Gaetani and Grove, 1997), and the latter to be 500 ppm, typical of high-MgO Chukotat basalt. The calculated R-factors associated with the high-tenor and low-tenor samples are highly sensitive to D_{Ni}, but the factor relating one R-factor to the other is relatively insensitive. Over the range $D_{Ni} = 500$ to 5000, the high and low tenor samples require R-factors that differ only by a factor of $2 - 3$, indicating that the events causing the formation of the nickel deposits increased the amount of sulphur in the system by this factor.

5.4 Implications for the magmatic history of the Raglan horizon

The nature and origin of the ultramafic units of the Raglan horizon have been debated by both academics and industry workers for some time. Originally thought to be the cumulate remains of choked magma sills that fed the early Chukotat basaltic flows (Barnes et al., 1982; Francis et al., 1983; Bédard et al., 1984), the ultramafic rocks have more recently been interpreted as the cumulate portions of lava flows (Barnes and Barnes, 1990). There is a wide range in opinion among Raglan geologists between these extremes. Although

field evidence for flow-tops exists and almost certainly confirms that some of the ultramafic units were extrusive, the bulk of the ultramafic units in the Raglan horizon display intrusive upper margins and we view the high-level sill interpretation as being generally the most useful. Any successful model must properly account for the fact that the parental liquids for all five sampled intersections were in equilibrium with an olivine of composition $\sim Fo_{89}$. Olivine-phyric Chukotat basalts that would be in equilibrium with Fo_{89} olivine (Fig. 8) range from the high-Si, low-Fe compositions that make up the bulk of the olivine-phyric basalts to rarer, low-Si, Fe-enriched examples. Although the calculated trapped liquid fields overlap the entire range of olivine-phyric Chukotat liquids, they strongly cluster at the high-Fe compositions (Fig. 9). The positive slope of the most magnesian olivine-phyric Chukotat basalts in Mg–Fe space (Fig. 8) was first noted by Francis et al. (1981), who proposed that both the positive slope and the compositional variability of these high-MgO basalts could be explained by a variation of 10 to 30% in the degree of adiabatic partial melting of the mantle, with the Fe-rich end-member representing the lowest degree of partial melting. These Fe-rich basalts are restricted to the lowermost cycle of Chukotat volcanism (Francis et al., 1981), which is stratigraphically immediately above the sills of the Raglan horizon. The olivine-phyric basalts of all the higher cycles are Fe-poor and Si-rich.

The Fe-rich picrites of the lower Chukotat have characteristics favourable to the formation of Ni-Cu-(PGE) deposits:

(1) As the first erupted products of Chukotat volcanism, the Fe-rich picrites intruded significant amounts black siltstone. These sediments are ubiquitously associated with the Raglan horizon sills, and are far less common in both the Upper Povungnituk and Chukotat formations. These early lavas

therefore experience greater exposure to crustal sulphur sources than the later ones.

(2) Melts formed from lower degrees of adiabatic partial melting of a mantle source region are expected to have higher temperatures. This can be graphically illustrated by use of the 'sail' diagrams of Hanson and Langmuir (1978), which show liquids capable of coexisting with a given mantle composition. In Mg–Fe space, the isotherms on such a diagram have small negative slopes, with temperature increasing towards more Mg-rich compositions. Curves of equal degree of partial melting have a pronounced positive slope. Liquids produced by adiabatic partial melting will define an array with a shallow positive slope, from higher to lower temperatures and higher degrees of partial melting with ascent. The array defined by the most magnesian olivine-phyric Chukotat liquids in such a diagram could be explained by this process, with the rare Fe-rich basalts representing the lowest degrees of partial melting and the highest temperature (Francis et al., 1981).

The calculated liquidus temperature for the Fe-rich end-member of the olivine-phyric Chukotat basalt suite is $\sim$ 90°C greater than that of the Fe-poor end-member (calculated using MELTS, Ghiorso and Sack, 1995). Higher temperature magmas are more likely to interact with crustal material because of their higher heat content and greater turbulence (Arndt et al., 2005), as well as have increased sulphur solubilities. Increasing FeO contents in particular has been shown to significantly increase sulphur solubilities (Haughton et al., 1974). The Fe-rich Chukotat picrites should have a greater ability to assimilate sulphur-rich sediments and segregate immiscible sulphide melts.

(3) The concentrations of both sulphur and the chalcophile elements in the

Fe-rich picrites are expected to differ from the Fe-poor picrites depending on whether sulphide has been melted out completely in the source or not. Assuming that sulphide is melted out in both cases (a reasonable assumption, since if any sulphide restite remained the PGE concentrations in the deposits would likely not be of ore grade, given the strongly chalcophilic behaviour of these elements), the Fe-rich picrites should have higher concentrations of sulphur and incompatible chalcophile elements (Cu, Pt-group PGE) and slightly lower concentrations of compatible chalcophile elements (Ni, Ir-group PGE) (Arndt et al., 2005).

6 Conclusions

We have shown that the data indicate the existence of parental liquids with the composition of the Fe-rich olivine-phyric Chukotat basalts and in equilibrium with olivine of $\sim Fo_{89}$. The Fe-rich olivine-phyric Chukotat basalts are restricted to the lowermost Chukotat volcanic cycle and are stratigraphically juxtaposed to the Raglan horizon. They appear to represent a smaller degree of adiabatic partial melting in the mantle than that responsible for the majority of the Chukotat basalts.

Both the olivine and whole-rock compositions record evidence of the segregation of sulphide liquid. Nickel tenors are lower in samples that record sulphide segregation, than in samples that do not, consistent with the proposal that addition of sulphur through the assimilation of sediments is required to saturate the magmatic system with respect to sulphur.

Fe-rich picrites are also associated with magmatic sulphide deposits in the

early Proterozoic Pechenga volcano-sedimentary belt, Russia (Naldrett, 2004, Ch. 5), and are there interpreted as requiring a different mantle source melting regime than that which produced associated tholeitic basalts. We suggest that there is also an association between the Fe-rich picrites of the lower Chukotat and the Ni-Cu-(PGE) deposits of the Raglan horizon. If Fe-rich picrites can be linked to magmatic sulphide deposits more generally, the search for these Fe-rich picrites may constitute a worthwhile mineral exploration criterion.

7 Acknowledgments

The authors wish to acknowledge Goldbrook Ventures Inc. for permission to use their compilation map of the public domain total magnetic intensity data (Fig. 1), and Phil Vicker and Falconbridge Limited for logistical and financial support. This research has also been supported by the Canadian National Science and Engineering Research Council (NSERC) grant # RGPIN 7977-00.

References

Arndt, N.T., Lesher, C.M., Czamanske, G.K., 2005. Mantle-derived magmas and magmatic Ni-Cu-(PGE) deposits. Economic Geology, 100th Anniversary volume, 5–24.

Barnes, S.-J., Coats, C.J.A., Naldrett, A.J., 1982. Petrogenesis of a Proterozoic nickel-sulfide-komatiite association; the Katiniq Sill, Ungava, Quebec. Economic Geology 77, 413–429.

Barnes, S.J., 1986. The effect of trapped liquid crystallization on cumulus mineral compositions in layered intrusions. Contributions to Mineralogy and Petrology 93, 524–531.

Barnes, S.J., Barnes, S.-J., 1990. A new interpretation of the Katiniq nickel deposit, Ungava, northern Quebec. Economic Geology 85, 1269–1272.

Beattie, P., Ford, C., Russell, D., 1991. Partition coefficients for olivine-melt and orthopyroxene-melt systems. Contributions to Mineralogy and Petrology 109, 212–224.

Bédard, J.H., Francis, D.M., Hynes, A.J., Nadeau, S., 1984. Fractionation in the feeder system of a Proterozoic rifted margin. Canadian Journal of Earth Science 21, 489–499.

Bégin, N., 1989. P-T conditions of metamorphism inferred from the metabasites of the Cape Smith Belt, northern Quebec. Geoscience Canada 16, 151–154.

Campbell, I.H., Naldrett, A.J., 1979. The influence of silicate:sulfide ratios on the geochemistry of magmatic sulfides. Economic Geology 74, 1503–1505.

Cawthorn, R.G., Sander, B.K., Jones, I.M., 1992. Evidence for the trapped liquid shift effect in the Mount Ayliff Intrusion, South Africa. Contributions to Mineralogy and Petrology 111, 194–202.

Francis, D.M., Hynes, A.J., Ludden, J.N., Bédard, J., 1981. Crystal fractionation and partial melting in the petrogenesis of a Proterozoic high-MgO volcanic suite, Ungava, Québec. Contributions to Mineralogy and Petrology 78, 27–36.

Francis, D.M., Ludden, J., Hynes, A.J., 1983. Magma evolution in a Proterozoic rifting environment. Journal of Petrology 24, 556–582.

Gaetani, G.A., Grove, T.L., 1997. Partitioning of moderately siderophile elements among olivine, silicate melt, and sulfide melt: Constraints on core formation in the Earth and Mars. Geochimica et Cosmochimica Acta 61, 1829–1846.

Ghiorso, M.S., Sack, R.O., 1995. Chemical Mass Transfer in Magmatic Processes IV. A revised and internally consistent thermodynamic model for the interpolation and extrapolation of liquid-solid equilibria in magmatic systems at elevated temperatures and pressures. Contrib Mineral Petrol 119, 197–212.

Giovenazzo, D., Picard, C., Guha, J., 1989. Tectonic setting of Ni-Cu-PGE deposits in the central part of the Cape Smith Belt. Geoscience Canada 16, 134–136.

Hanson, G.N., Langmuir, C.H., 1978. Modelling of major elements in mantle-melt systems using trace element approches. Geochimica et Cosmochima Acta 42, 725–741.

Haughton, D.R., Roeder, P.L., Skinner, B.J., 1974. Solubility of sulfur in mafic magmas. Economic Geology 69, 451–467.

Hynes, A.J., Francis D.M., 1982. A transect of the early Proterozoic Cape Smith foldbelt, New Quebec. Tectonophysics 88, 23–59.

Keayes, R.R., 1995. The role of komatiitic and picritic magmatism and S-saturation in the formation of ore deposits. Lithos 34, 1–18.

Lundgaard, K.L., Tegner, C., Cawthorn, R.G., Kruger, F.J., Wilson, J.R., 2006. Trapped intercumulus liquid in the Main Zone of the eastern Bushveld Complex, South Africa. Contributions to Mineralogy and Petrology 151, 352–369.

Machado N., Gariépy, C., Philippe, S., David, J., 1990. Géochronologie U–Pb du territoire Québecois: Fosses du Labrador et de l'Ungava et sous-province de Pontiac: Premier rapport intérimaire: Résultats 1989–90, GEOTOP, Université du Québec à Montréal, 25–39.

Maier, W.D., Barnes, S.-J., de Waal, S.A., 1998. Exploration for magmatic Ni–Cu–PGE sulphide deposits: a review of recent advances in the use of geochemical tools, and their application to some South African ores. South African Journal of Geology 101, 237–253.

Maurel, C., Maurel, P., 1982. Etude expérimentale de l'équilibre Fe^{2+}–Fe^{3+} dans les spinelles chromifères et les liquides silicatés basiques. Comptes Rendus Hebdomadaires des Séances de l'Académie des Sciences II-295, 209–212.

Modeland, S., Francis, D., Hynes, A., 2003. Enriched mantle components in Proterozoic continental-flood basalts of the Cape Smith foldbelt, northern Québec. Lithos 71, 1–17.

Naldrett, A.J., Duke, J.M., Lightfoot, P.C., Thompson, J.F.H., 1984. Quantitative modelling of the segregation of magmatic sulphides: an exploration guide. Canadian Institute of Mining Bulletin 77 (864), 46–56.

Naldrett, A.J., 2004. Deposits of the Pechenga area, Russia. In: Magmatic Sulfide Deposits – Geology, Geochemistry and exploration. Springer–Verlag, Berlin, 279–306.

Parrish, R.R., 1989. U-Pb geochronology of the Cape Smith Belt and Sugluk block, northern Quebec. Geoscience Canada 16, 126–130.

Pearce, T.H., 1968. A contribution of the theory of variation diagrams. Con-

tributions to Mineralogy and Petrology 19, 142–157.

Picard, C., Lamothe, D., Piboule, M., Oliver, R., 1990. Magmatic and geotectonic evolution of a Proterozoic oceanic basin: The Cape Smith Thrust-Fold Belt (New Quebec). Precambrian Research 47, 223–249.

Roeder, P.L., Emslie, R.F., 1970. Olivine-liquid equilibrium. Contributions to Mineralogy and Petrology 29, 275–289.

St-Onge, M.R., Lucas, S.B., Parrish, R.R., 1992. Terrane accretion in the internal zone of the Ungava Orogen, northern Québec; Part I, Tectonostratigraphic assemblages and their tectonic implications. Canadian Journal of Earth Sciences 29, 746–764.

St-Onge, M.R., Lucas, S.B., 1993. Geology of the eastern Cape Smith belt: Parts of the Kangiqsujuaq, Cratère du Nouveau-Québec, and Lacs Nuvilik map areas, Quebec. Geological Survey of Canada Memoir 438.

Stewart, A.J., 2002. The geochemistry and physical volcanology of the East Lake ultramafic zone, Cape Smith belt, northern Quebec. M.Sc. thesis, McGill University.

Table 1

Representative whole-rock and olivine analyses, and normative mineralogy. Core samples were analysed for major elements and selected trace elements by X-ray fluorescence (XRF) spectrometry at SGS Lakefield Research, Lakefield, Ontario, Canada. The olivines were analysed for major elements with a JEOL8900 electron microprobe at McGill University, using an accelerating voltage of 20 kV and a beam current of 30 nA, with counting times of 60 seconds on peak and background for Ni and Ca, 20 seconds for the other elements. Natural and synthetic standards were used for calibration with ZAF correction procedure. Total iron in the whole-rock analyses is reported as Fe_2O_3.

Sample		A648	A673	A683	B404	B484	B509	C963	C982	C1002	D49	D67	E4	E15
Whole rock														
SiO_2	%	35.4	36.9	37.4	37.6	37.4	37.2	39.1	39.3	38.1	39.9	39.6	40.8	40.2
Al_2O_3	%	2.31	2.36	2.55	2.38	2.44	2.09	2.25	2.27	2.40	3.04	3.05	4.88	5.03
Fe_2O_3	%	12.6	11.8	11.7	13.1	11.1	12.7	14.3	14.4	15.6	12.6	12.0	13.5	13.4
MgO	%	34.9	35.9	36.5	36.3	37.9	37.8	39.0	39.5	37.1	35.6	35.7	30.0	29.6
CaO	%	1.46	2.03	1.74	1.81	1.42	2.04	2.26	2.07	2.85	3.03	2.98	4.63	4.75
Na_2O	%	< 0.05	0.10	0.06	< 0.05	0.07	< 0.05	0.10	0.07	0.10	0.12	0.06	0.29	0.32
K_2O	%	0.03	0.08	0.27	0.04	0.04	0.03	0.15	0.16	0.14	0.26	0.19	0.27	0.35
TiO_2	%	0.46	0.25	0.15	0.15	0.13	0.11	0.13	0.13	0.13	0.21	0.18	0.29	0.29
P_2O_5	%	0.01	0.01	< 0.01	0.01	< 0.01	0.01	< 0.01	0.01	0.01	0.02	0.02	0.03	0.02
MnO	%	0.20	0.15	0.16	0.17	0.15	0.16	0.17	0.16	0.18	0.19	0.17	0.22	0.20
Cr_2O_3	%	0.66	0.66	0.71	0.64	0.73	0.73	0.73	0.76	0.76	0.74	0.76	0.47	0.46
V_2O_5	%	0.02	0.01	0.02	0.01	0.01	< 0.01	0.01	0.01	0.01	< 0.01	0.01	0.02	0.02
LOI	%	10.30	8.72	7.76	7.80	7.20	5.98	2.35	1.91	1.86	5.87	6.10	5.65	5.57
Total	%	98.4	98.9	99.0	100.0	98.6	98.9	100.5	100.7	99.2	101.5	100.8	101.1	100.3
Ba	ppm	23	< 10	32	< 10	< 10	< 10	23	12	19	28	23	11	37
Sr	ppm	< 5	< 5	8	< 5	< 5	< 5	11	11	11	20	13	47	42
Y	ppm	< 5	< 5	< 5	< 5	< 5	< 5	<5	< 5	< 5	< 5	< 5	< 5	6
Zr	ppm	20	10	16	10	9	6	8	6	8	16	12	21	18
Ni	ppm	2540	2140	1680	2770	2030	4790	3810	4080	5250	1470	1690	1290	1310
Cu	ppm	257	284	114	215	30	906	567	501	1163	12	18	91	112
Co	ppm	136	136	134	136	127	176	204	202	225	120	129	112	114
Au	ppb	9	9	7	19	7	20	25	24	34	< 5	< 5	< 5	< 5
Pt	ppb	16	18	7	39	6	70	68	56	89	< 5	8	< 5	9
Pd	ppb	49	57	28	98	15	181	159	133	151	< 5	7	< 5	12
S	%	0.42	0.35	0.34	0.28	0.04	0.81	1.08	1.08	1.94	0.03	0.01	0.01	0.02
Olivine														
SiO_2	%	39.34	39.47	39.92	39.39	39.62	39.62	39.30	39.15	39.34	39.39	39.60	38.96	38.94
Al_2O_3	%	0.05	0.04	0.04	0.05	0.05	0.05	0.04	0.06	0.03	0.04	0.03	0.03	0.03
FeO	%	11.93	11.85	11.68	14.38	12.05	12.29	12.23	12.08	12.73	13.74	13.21	16.53	16.45
MgO	%	47.71	47.38	47.34	45.25	47.08	47.01	47.43	47.46	46.98	45.87	46.20	43.73	43.80
CaO	%	0.26	0.25	0.21	0.24	0.22	0.18	0.24	0.25	0.22	0.16	0.15	0.17	0.20
TiO_2	%	0.01	0.01	0.00	0.01	0.01	0.00	0.01	0.00	0.01	0.01	0.01	0.01	0.01
MnO	%	0.18	0.17	0.17	0.19	0.18	0.18	0.18	0.18	0.19	0.21	0.19	0.24	0.24
Cr_2O_3	%	0.05	0.04	0.04	0.04	0.05	0.03	0.04	0.04	0.03	0.02	0.02	0.02	0.02
Total	%	99.53	99.21	99.42	99.56	99.24	99.36	99.47	99.22	99.52	99.44	99.41	99.68	99.69
Ni	ppm	1573	1474	1170	2186	2270	2128	1338	1528	1551	1833	2103	2019	1983
Normative mineralogy														
Oliv	%	76.4	76.1	76.3	76.3	80.3	79.0	77.8	78.2	73.6	71.1	71.0	58.2	59.6
Cpx	%	0.8	3.5	2.0	2.2	0.6	3.8	4.5	3.6	6.5	6.1	5.7	9.0	9.4
Opx	%	10.4	8.7	9.5	10.6	8.6	5.7	5.0	5.5	4.1	10.1	10.9	14.6	11.9
Feld	%	7.1	7.3	7.4	7.0	7.4	6.1	6.2	6.2	6.7	8.6	8.7	14.3	14.8
Cr	%	1.1	1.1	1.2	1.0	1.2	1.2	1.1	1.1	1.2	1.2	1.2	0.7	0.7
Mt	%	1.7	1.5	1.5	1.7	1.4	1.6	1.7	1.7	1.9	1.6	1.5	1.7	1.7
Po	%	1.3	1.1	1.0	0.8	0.1	2.4	3.0	3.0	5.5	0.1	0.0	0.0	0.1
Im	%	1.0	0.5	0.3	0.3	0.3	0.2	0.3	0.3	0.3	0.4	0.4	0.6	0.6

Fig. 1. Location map for the drill holes sampled in this study. The drill sections are referred to as A through E and represent DDHs 718-1000, 718-1260, 718-1007, 718-949, and 909-09, respectively. On this map of total magnetic intensity, the serpentinized sills of the Raglan horizon figure as prominent magnetic highs, and the horizon is easy to trace as a strike parallel series of discontinuous sills. Magnetic data from public domain Quebec government statutory mineral exploration company reports.

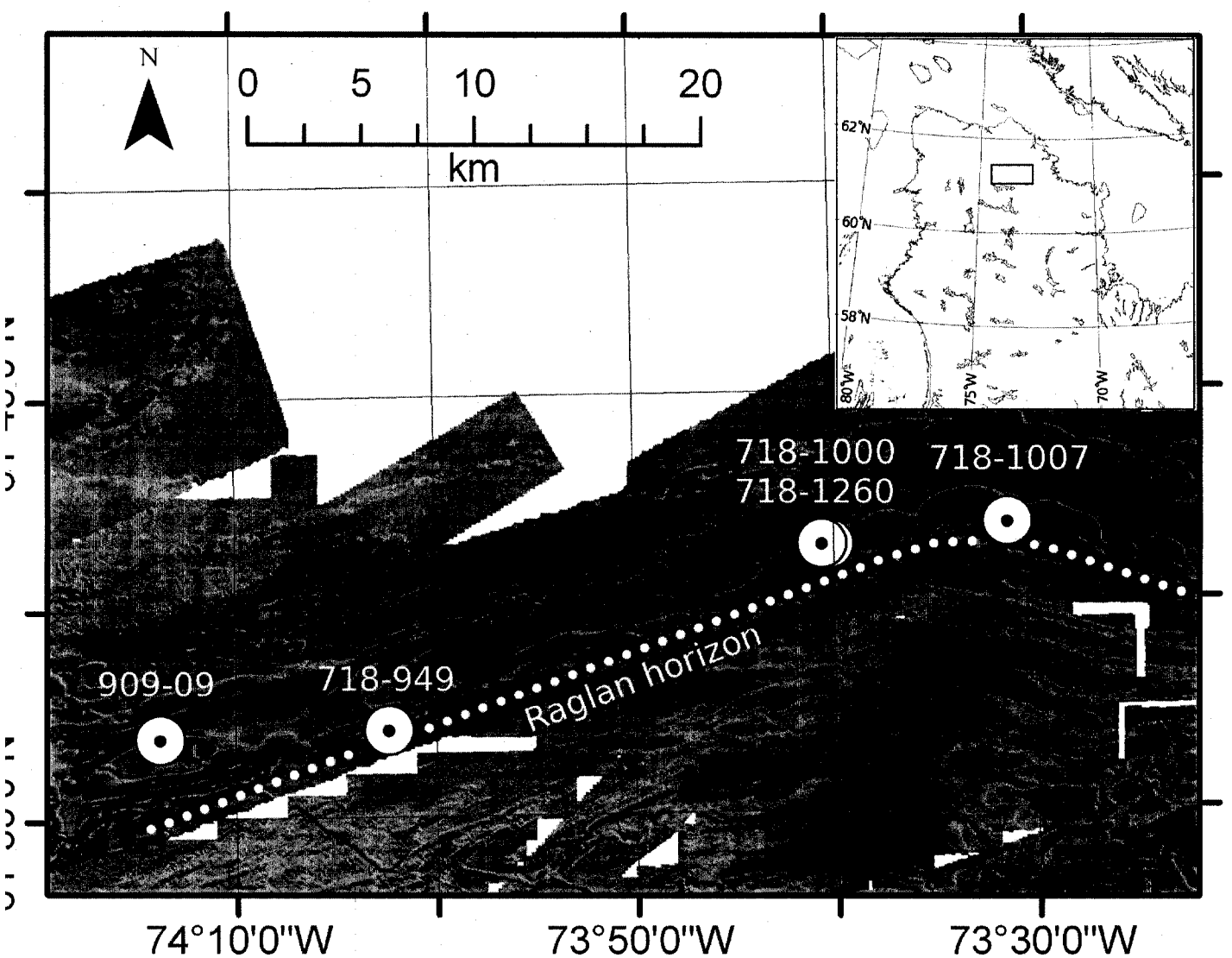
N
0
5
10
20
km
62°N
60°N
58°N
80°W
75°W
70°W
718-1000
718-1260
718-1007
909-09
718-949
Raglan horizon
74°10'0"W
73°50'0"W
73°30'0"W

Fig. 2. Scanning electron photomicrograph of an unaltered ultramafic cumulate from section A, showing euhedral olivine and chromite in a fine-grain serpentinzed matrix. Fresh interstitial pyroxene is occasionally present. Scale is shown in lower left hand corner of the image; the white bar is 500 microns.

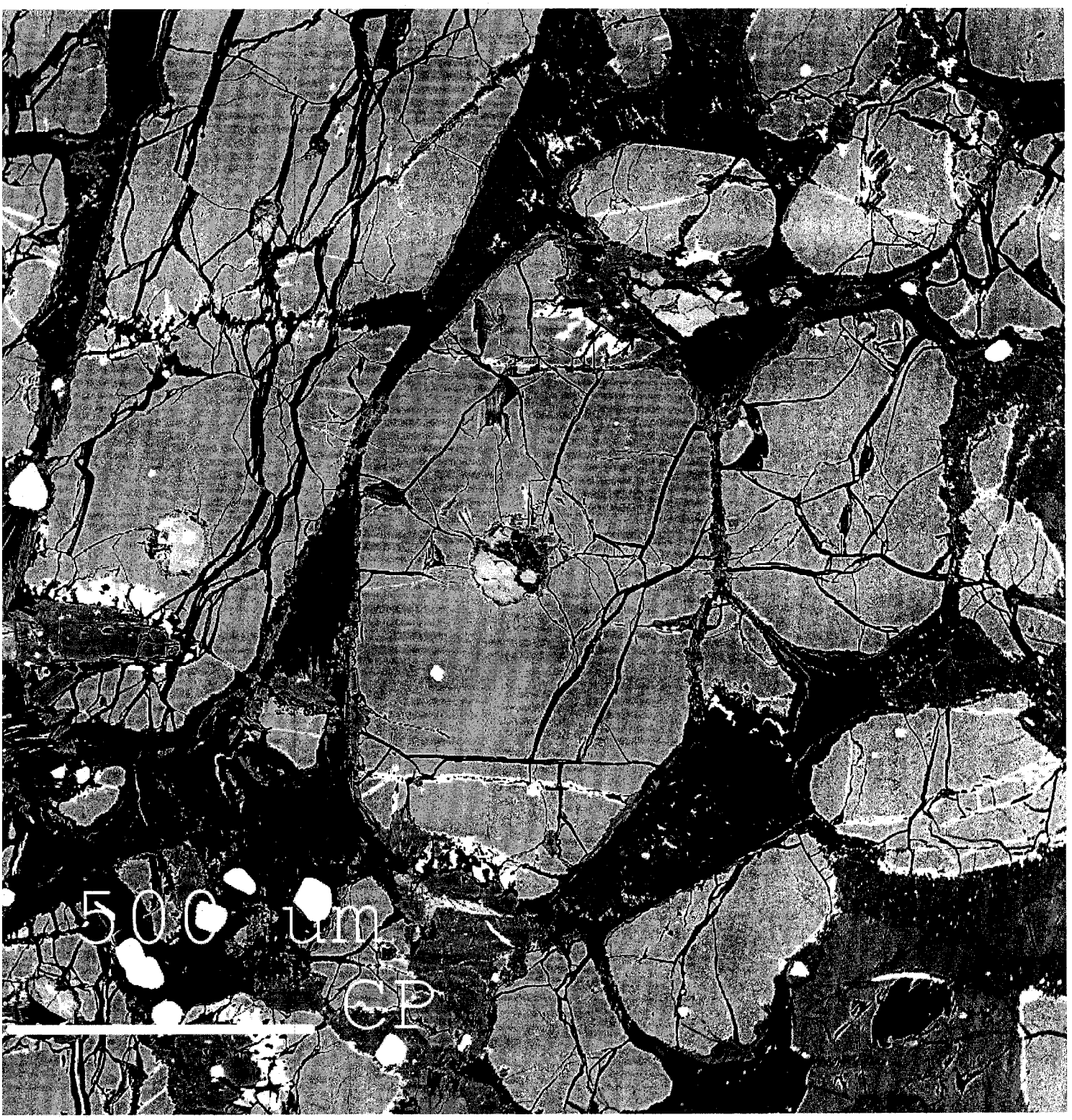
500 um
CP

Fig. 3. Whole-rock and olivine nickel and $Mg^{\#}$ plotted against drill hole depth and sill lithology for four of the drill holes in this study. The sections correspond to DDH #s as follows: Section A, DDH 718-1000; section B, DDH 718-1260; section C, DDH 718-1007; section D, DDH 718-949. Section E is not shown in the figure but corresponds to DDH 909-09. Symbols: whole-rock compositions, shaded squares; olivine compositions, white diamonds; sulphur-corrected silicate fraction of the whole-rock compositions, black squares. The Falconbridge Ltd. drill log lithology is graphically represented as a function of hole depth between the $Mg^{\#}$ and Ni diagrams. Symbols: peridotite, cross-hatched pattern; pyroxenitic peridotite, right-leaning diagonal stripes; pyroxenite, left-leaning diagonal stripes; footwall melanogabbro, black mottled pattern.

a) Section A

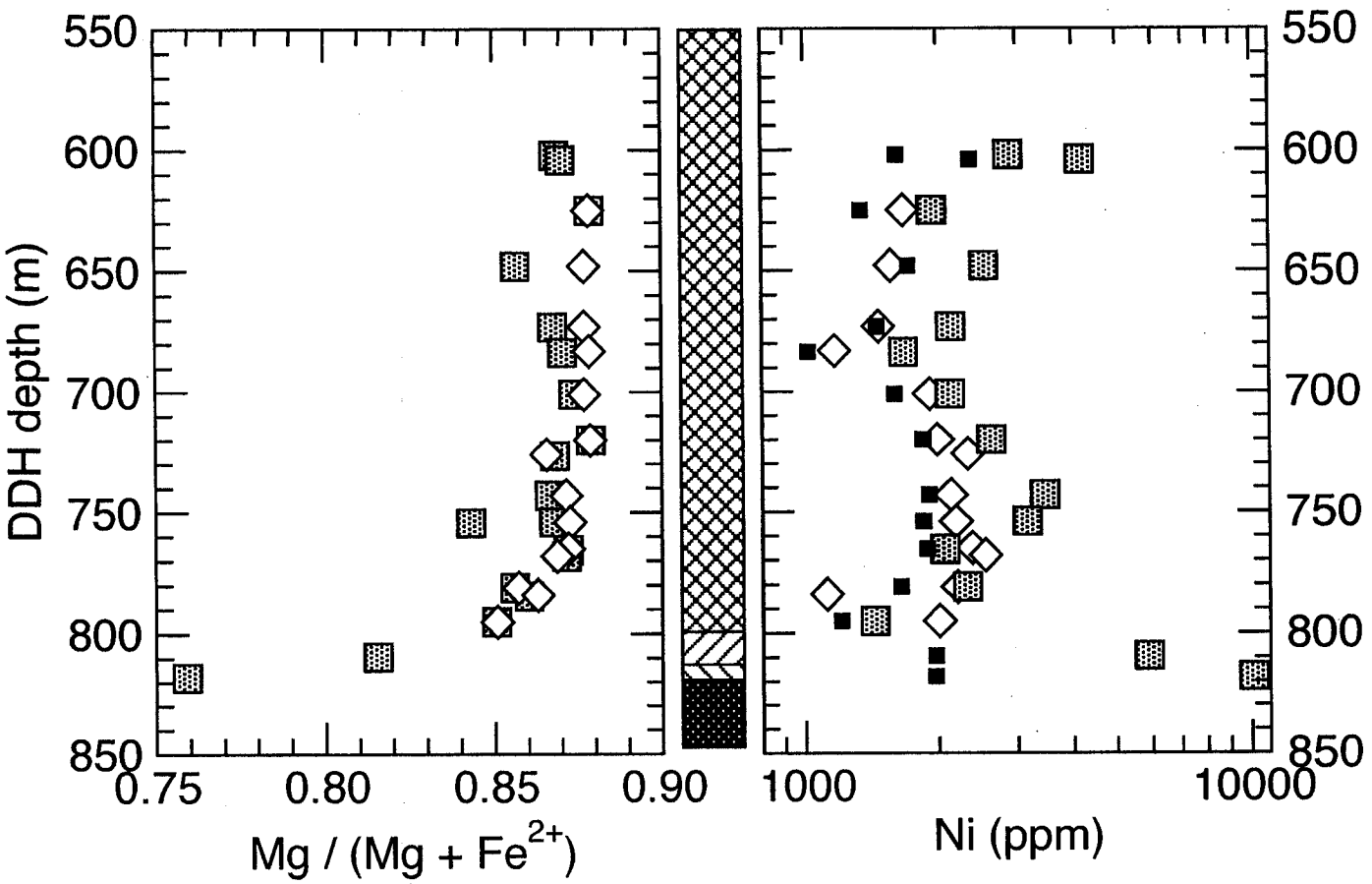
550
600
650
700
750
800
850
DDH depth (m)
0.75
0.80
0.85
0.90
Mg / (Mg + Fe2+)
1000
10000
Ni (ppm)

b) Section B

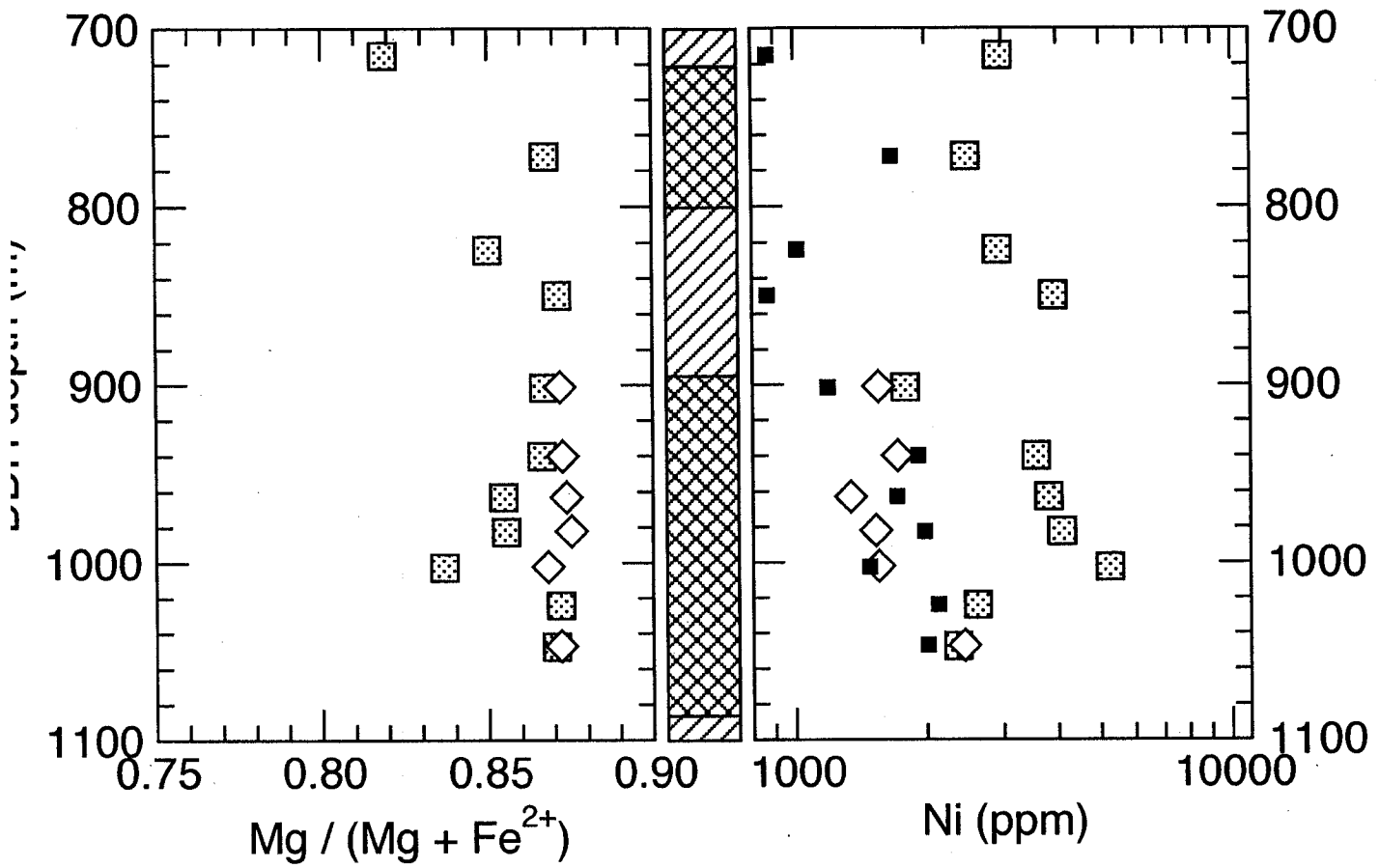
700
800
900
1000
1100
0.75
0.80
0.85
0.90
1000
10000
Mg / (Mg + Fe2+)
Ni (ppm)

c) Section C

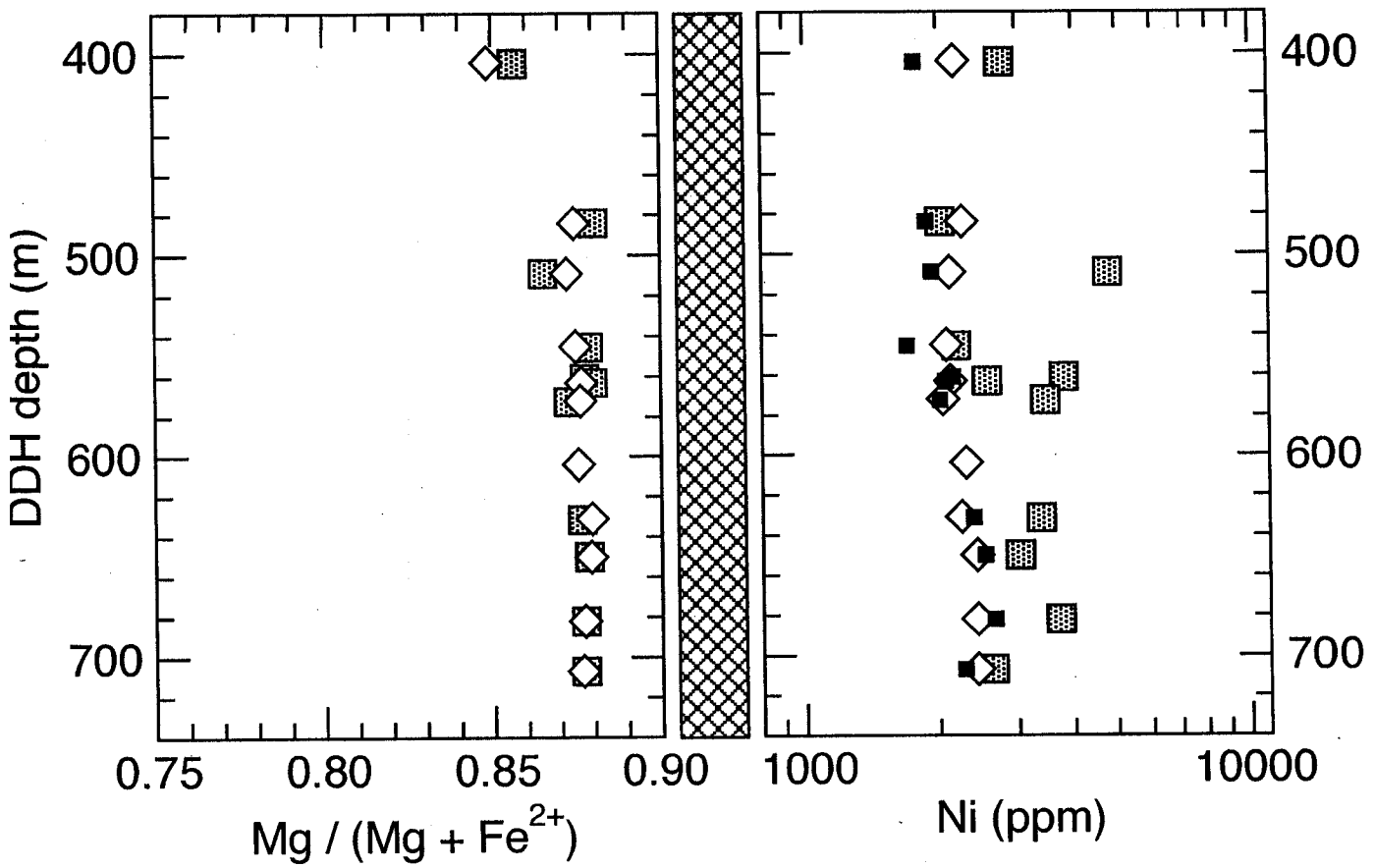
400
500
600
700
DDH depth (m)
0.75
0.80
0.85
0.90
Mg / (Mg + Fe2+)
1000
10000
Ni (ppm)

d) Section D

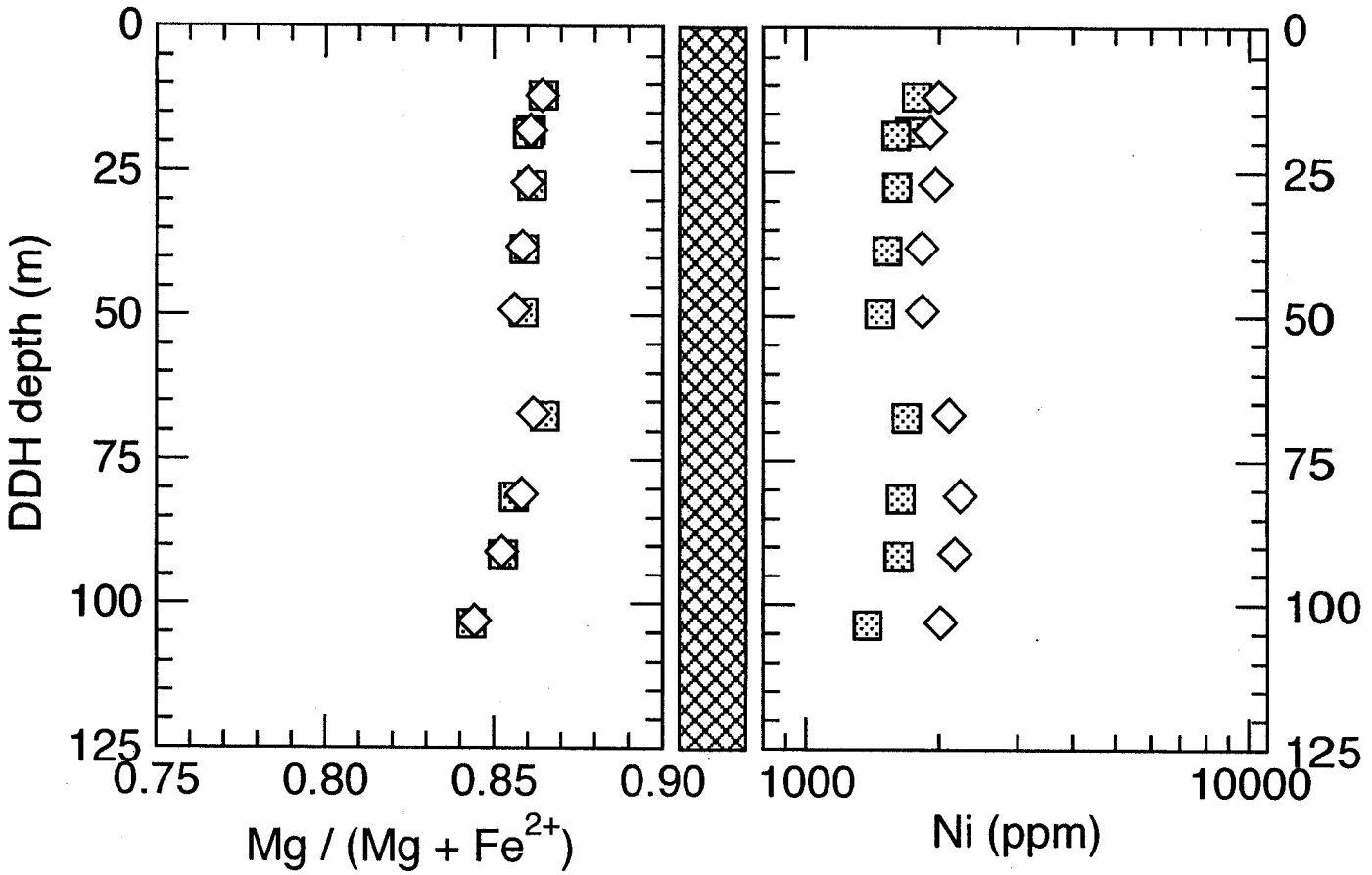
DDH depth (m)
0
25
50
75
100
125
0.75
0.80
0.85
0.90
Mg / (Mg + Fe2+)
1000
10000
Ni (ppm)

Fig. 4. Ni (ppm) versus Mg / (Mg + Fe) for olivine analyses presented in this study. The upper curve is an equilibrium crystallization curve for olivine crystallizing from a model olivine-phyric Chukotat basalt parental liquid, calculated using the partition coefficients of Beattie et al. (1991). The lower curve is a schematic representation of the effect of separating a sulphide liquid from the silicate. Symbols: section A, shaded circles; section B, inverted shaded triangles; section C, upright triangles; section D, squares; section E, +

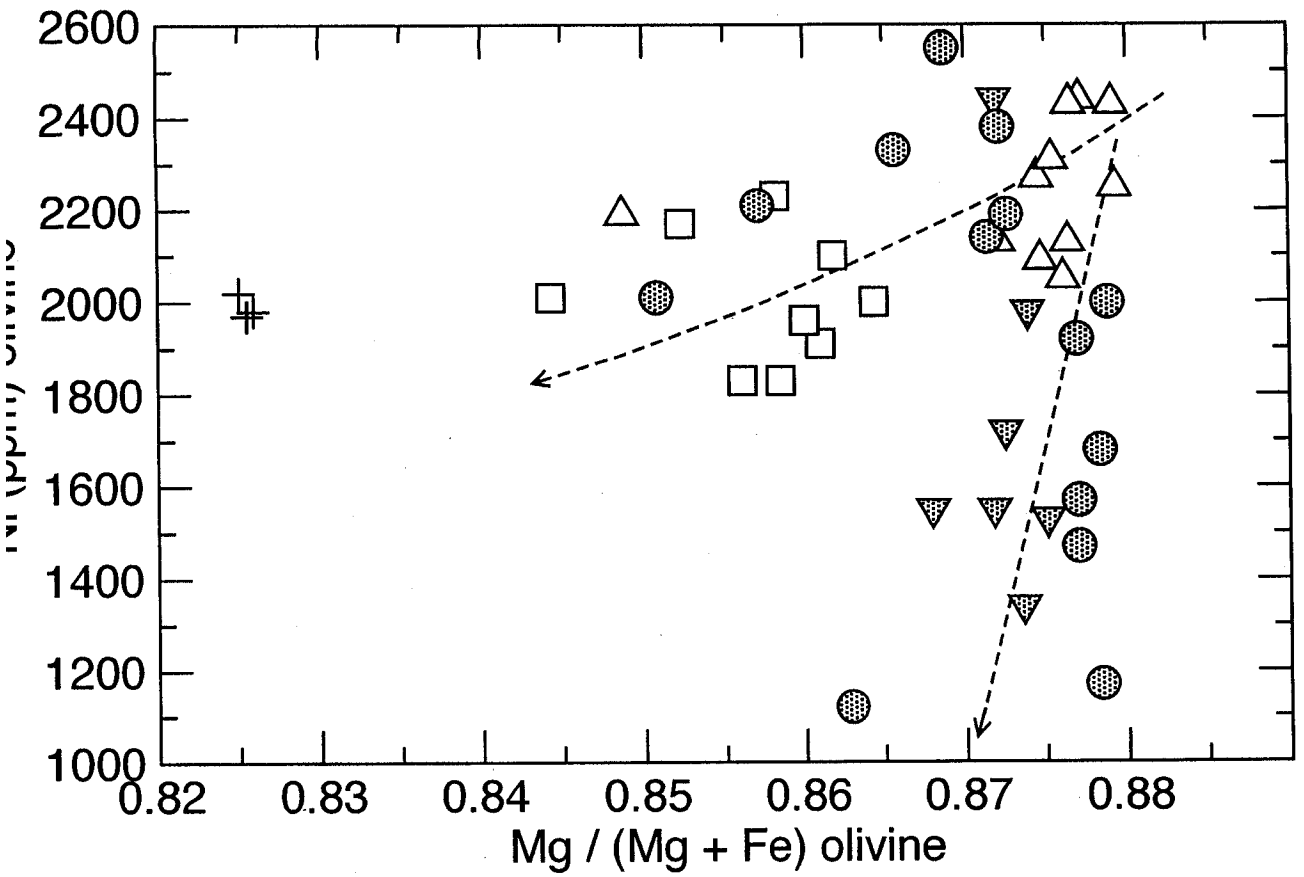
2600
2400
2200
2000
1800
1600
1400
1200
1000
0.82
0.83
0.84
0.85
0.86
0.87
0.88
Mg / (Mg + Fe) olivine

Fig. 5. Ni (ppm) versus S (wt%) for the whole-rock analyses. Symbols as in Fig. 4. The solid lines are mixing lines between undepleted olivine and high-tenor massive ore, and between depleted olivine and low-tenor massive ore. The data that fall on the shallower mixing line are equivalent to those on the steeper trend in Fig. 4. The mixing lines and tenors were determined by regressing the two sample populations (> 0.1% S) and extrapolating to 39 wt% S. Correlation coefficients for the regressions are 0.985 for the 13.5% Ni line and 0.952 for the 7.5% Ni line. Whole-rock silicate nickel contents can be estimated by extrapolating whole-rock Ni concentrations to 0% S along the mixing line appropriate to a given sample.

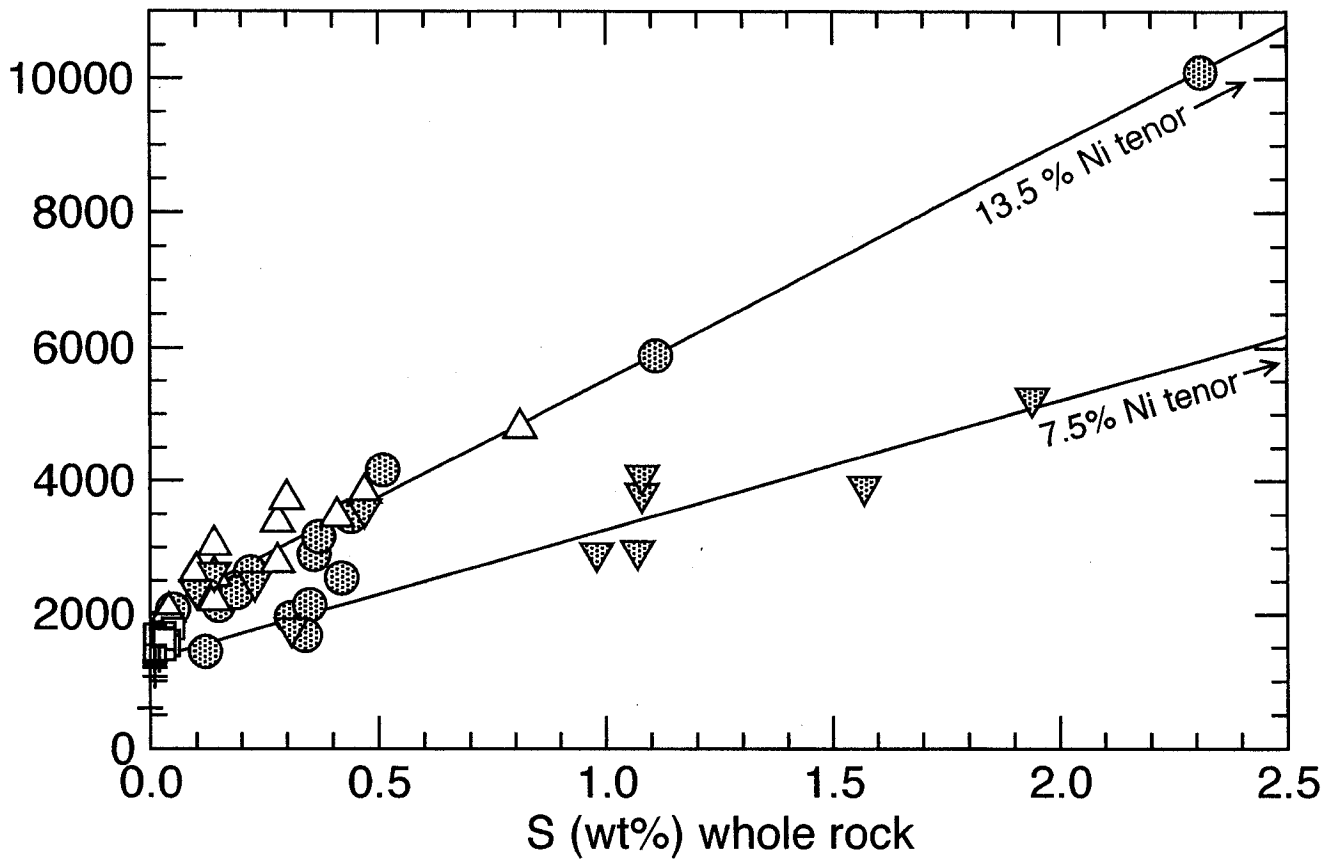
10000
8000
6000
4000
2000
0
0.0
0.5
1.0
1.5
2.0
2.5
S (wt%) whole rock
13.5 % Ni tenor
7.5% Ni tenor

Fig. 6. (Mg + Fe^{2+}) versus Si cation units for ultramafic cumulate whole-rock chemistry and Chukotat olivine-phyric basalts. Symbols: olivine-phyric Chukotat basalt, small diamonds, other symbols as in Fig. 4

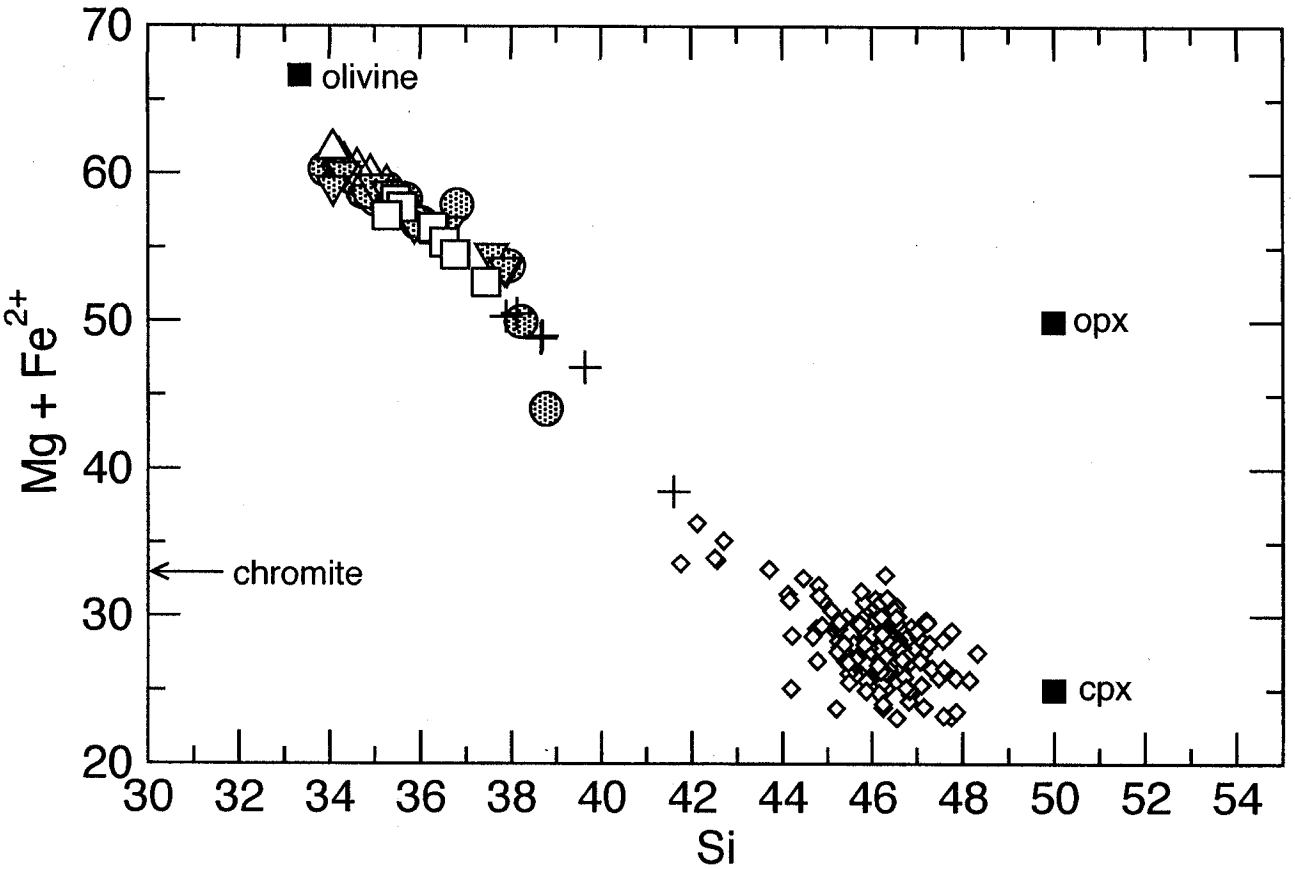
olivine
opx
cpx
chromite
Mg + Fe2+
Si
70
60
50
40
30
20
30
32
34
36
38
40
42
44
46
48
50
52
54

Fig. 7. Pearce element-ratio diagram showing (Mg + Fe) / Ti versus Si / Ti in cation units for the whole-rock analyses presented in this study. Data has been filtered to remove samples with S > 0.5%. Symbols are as in Fig. 4. Three hypothetical lines with slopes 0.5, 1 and 2 represent the effects of, respectively, clinopyroxene, orthopyroxene and olivine sorting. The cumulate data have a slope of 2.0056, a non-zero intercept of -117.3 and a correlation coefficient R of 0.998, indicating that olivine sorting is the only process involved in creating the geochemical variation shown here.

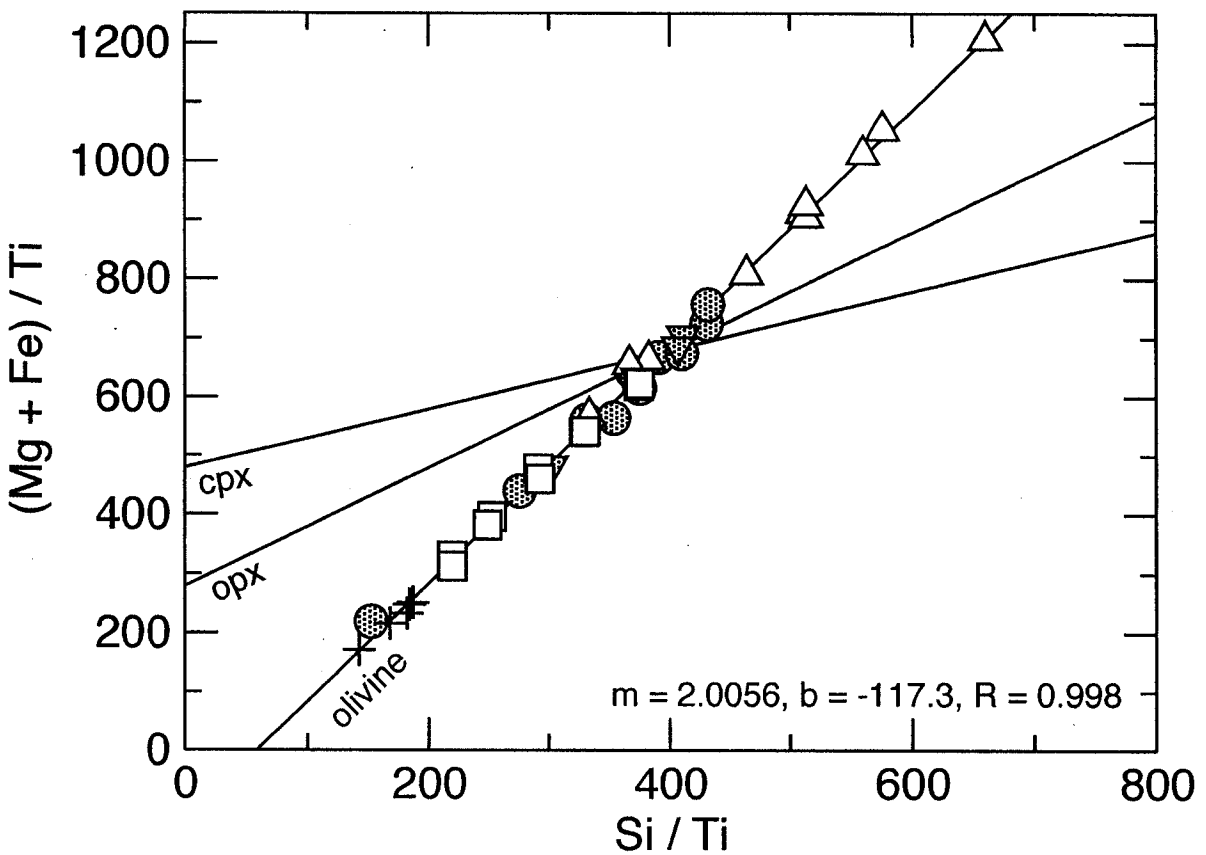
1200
1000
800
600
400
200
0
0
200
400
600
800
(Mg + Fe) / Ti
Si / Ti
cpx
opx
olivine
m = 2.0056, b = -117.3, R = 0.998

Fig. 8. Mg versus Fe^{2+} in cation units. Olivine and whole-rock data are shown, as well as the compositions of the olivine-phyric Chukotat basalts Francis et al. (1981). Lines represent the stoichiometric compositions of olivine, orthopyroxene and clinopyroxene; olivine compositions are represented by small black squares and labelled with Fo content. The data have been filtered to remove samples with $> 0.5\%$ S. Symbols as in Fig. 4.

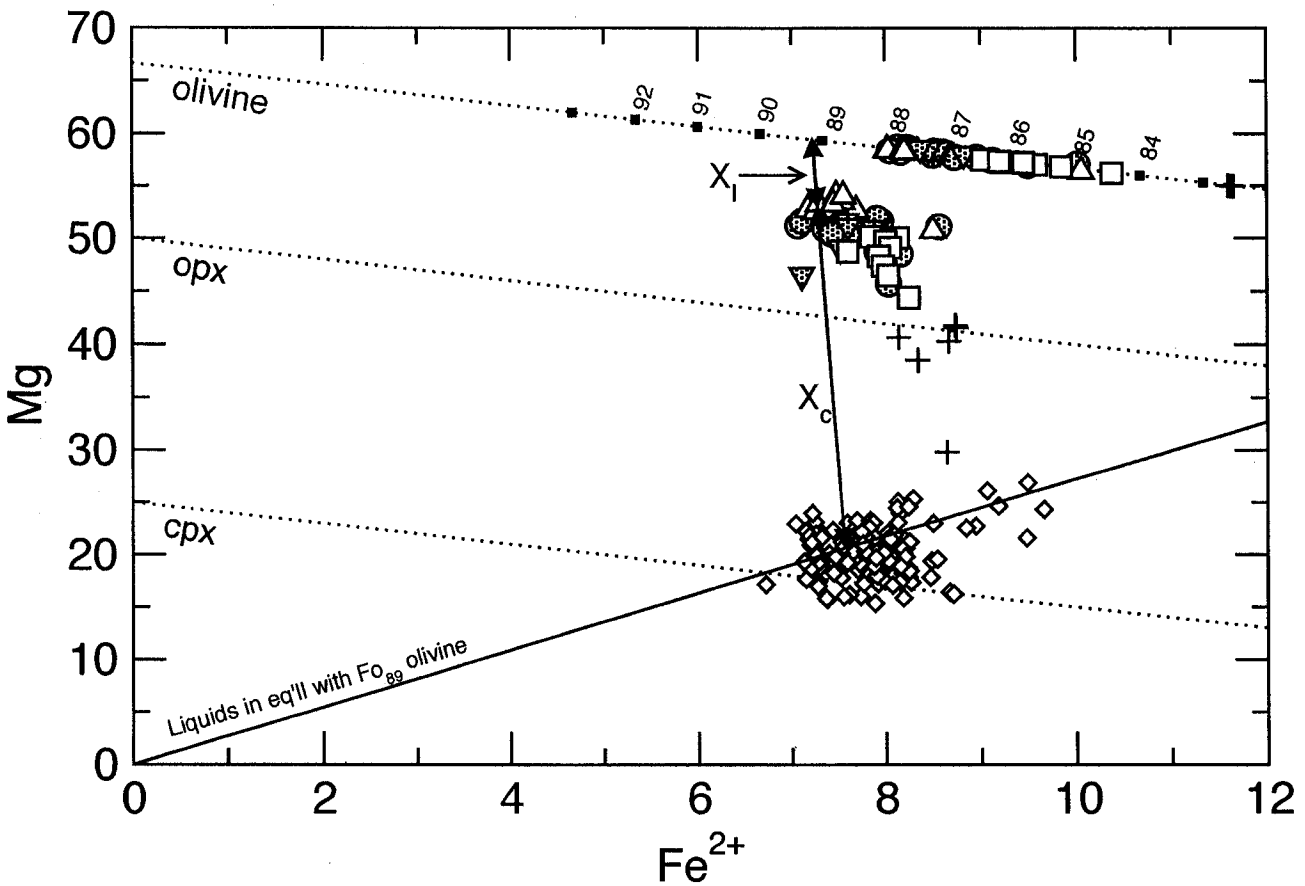
70
60
50
40
30
20
10
0
Mg
olivine
opx
cpx
92
91
90
89
88
87
86
85
84
X_l
X_c
Liquids in eq'll with Fo_{89} olivine
0
2
4
6
8
10
12
Fe^{2+}

Fig. 9. $Mg^{\#}$ versus Si in cation units for the ultramafic cumulates, olivine-phyric Chukotat basalts, and calculated liquids. Symbols: Cumulates, X; olivine-phyric Chukotat basalt, small diamonds; calculated cumulate interstitial liquids, circles. The spectrum of olivine compositions is represented by the labeled vertical line, located at Si = 33.3. The regression line through the cumulate data intersects the olivine line at $\sim Fo_{89}$.

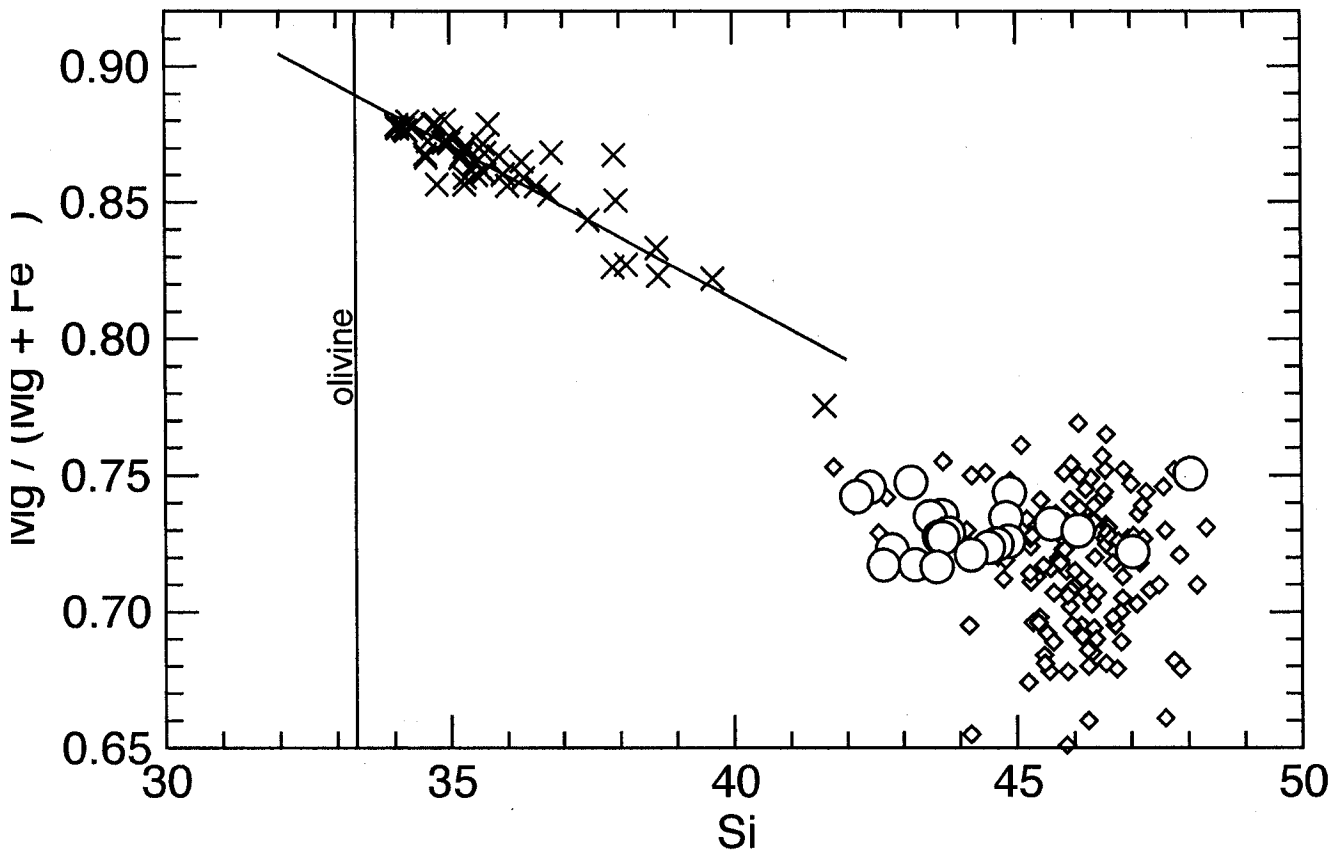
0.90
0.85
0.80
0.75
0.70
0.65
Mg / (Mg + Fe)
olivine
30
35
40
45
50
Si

4 Conclusions

This work is the first to suggest that the Raglan horizon ultramafic cumulates have parental liquids more Fe-rich than the bulk of the olivine-phyric Chukotat basalts. This result is significant because it offers an explanation for the presence of significant Ni-Cu-(PGE) deposits in the Raglan horizon that has not been previously considered. The assimilation of crustal sediments has often been suggested as being a necessary condition for sulphide segregation in the Raglan horizon. There are, however, many ultramafic sills in both the Chukotat and Povungnituk Groups that are unmineralized despite clear association with crustal sediment horizons. This work suggests that the Fe-rich picrites of the basal Chukotat Group may have had characteristics better suited to the segregation of sulphides than their later equivalents. Further work is required to test the Fe-rich parental liquid hypothesis using the compositions of ultramafic units in the barren horizons of the Cape Smith foldbelt.

Additionally, the Delta horizon (also referred to as the South Trend or Expo intrusive suite) in the Povungnituk Group is emerging as another significant nickel camp in the Cape Smith belt and has been interpreted as part of the same magmatic suite as the Raglan horizon (*Mungall, J.E., 2007. Crustal contamination of picritic magmas during transport through dikes: the Expo Intrusive Suite, Cape Smith fold belt, New Quebec. J. Petrol. 48, 1021–1039*). If this is the case, the sills of the Delta horizon should also require Fe-enriched parental magmas. Additional study of the sills of the Delta horizon may indicate if this is the case.

5 Acknowledgments

I would like to acknowledge Phil Vicker, formerly of Falconbridge Limited, for instigating this project, for providing logistical and financial assistance. Glenn Poirier, formerly of McGill University, assisted me in setting up, calibrating, and running the electron microprobe. Don Francis generously provided his venerable plotting software, and gave me the impetus to start writing my own.

Although I learned a lot about geology during the course of this M.Sc., I'm not certain that it was the most valuable part of the experience. The memories of my many interactions with the fine folks of this department and what I've learned about people and the place of science in society will long outlast any knowledge of olivine behaviour that I may have gained.

In particular, I'd like to thank Don Francis, Andrew Hynes, Jafar Arkani-Hamed and Olivia Jensen for your principled attitudes and clear (and uncompromising?) opinions on science and society. You have been a source of inspiration and have certainly helped shape my own world view.

I thank my office-mates and friends Jean-Francois Ravenelle, Simon Gagné, Fraser Keppie, and Andrew Hynes for providing such a warm and collegial environment in which to talk, think, work and drink.

Thank you to Anne Kosowski, Kristy Thornton, and Carol Matthews for bailing me out every time I ran afoul of McGill's bureaucracy. I appreciate very much all you have done and hope I've not been too much of a burden, or, failing that, that I've at least been a humorous burden.

Thank you to my parents for your support and love; thank you especially to my father for reading an earlier draft of this manuscript. Thank you also

to Maria Keane-Lara and family for your love and always open door and steady supply of frijoles.

Thank you to all my friends in EPS, past & present. You have all contributed to my experience here. Over the years a few individuals, either through their friendships or the significance of their contributions to my experience, have stood out particularly: (in chronological order) Sheldon Modeland, David Dolejs, J-F Ravenelle, Josh Gladstone, Joanne Garton, Surdas Mohit, Crystal Mann, Fraser Keppie, Robbie Gray & Jon Hanson. Special thanks to Andrew Jarjour, Ph.D., for many a late night pint and afternoons of mutually-enforced work. Apologies to anyone I've missed in my last minute scramble to write this.

Lastly, a special thank you to my supervisor Don Francis for your patience in enduring my several industry-related AWOL episodes, and your support, guidance, and forthrightness throughout.

Onwards...

A Whole-rock and olivine chemistry

WHOLE ROCK MAJOR ELEMENT XRF ANALYSES

Sample ID	SiO2 %	Al2O3 %	Fe2O3 %	MgO %	CaO %	Na2O %	K2O %	TiO2 %	P2O5 %	MnO %	Cr2O3 %	V2O5 %	LOI %	Sum %
Section A														
718-1000 602.0	38.1	2.58	11.4	34.9	1.11	0.13	0.06	0.15	0.01	0.14	0.65	0.02	10.3	99.5
718-1000 604.0	37.6	1.9	12.5	38.9	2.11	0.08	0.04	0.11	< 0.01	0.16	0.75	< 0.01	4.4	98.6
718-1000 625.0	37.4	2.51	10.7	36	2.12	0.08	0.04	0.14	0.01	0.15	0.7	< 0.01	9.76	99.7
718-1000 648.0	35.4	2.31	12.6	34.9	1.46	< 0.05	0.03	0.46	0.01	0.2	0.66	0.02	10.3	98.4
718-1000 673.0	36.9	2.36	11.8	35.9	2.03	0.1	0.08	0.25	0.01	0.15	0.66	0.01	8.72	98.9
718-1000 683.5	37.4	2.55	11.7	36.5	1.74	0.06	0.27	0.15	< 0.01	0.16	0.71	0.02	7.76	99
718-1000 701.0	38.9	2.46	11.8	37.9	3.08	0.1	0.14	0.12	< 0.01	0.17	0.73	0.02	4.39	99.8
718-1000 720.0	38.2	2.32	11.3	38.1	2.91	0.1	0.1	0.13	< 0.01	0.19	0.72	< 0.01	4.61	98.7
718-1000 743.0	38.8	2.47	12.9	38.9	1.91	0.1	0.32	0.14	0.01	0.17	0.72	0.01	3.28	99.7
718-1000 754.0	39	2.23	12.9	39.3	2.03	0.08	0.22	0.12	0.01	0.17	0.8	0.01	2.67	99.6
718-1000 765.5	39.2	2.69	12.2	38.6	2.34	0.21	0.25	0.14	0.01	0.17	0.78	0.01	2.79	99.4
718-1000 781.0	39.4	3.06	12.9	35.6	2.69	0.17	0.39	0.19	0.02	0.17	0.63	0.02	4.32	99.6
718-1000 795.0	40.2	3.04	12.3	32.5	3.45	0.2	0.29	0.35	0.03	0.18	0.62	0.02	6.3	99.4
718-1000 809.5	39.3	5.37	13.7	28.1	3.79	0.15	0.15	0.26	< 0.01	0.17	0.5	0.02	8.61	100.1
718-1000 818.0	38.9	7.47	15.4	22.5	5.66	0.19	0.18	0.42	0.03	0.2	0.42	0.03	6.51	97.9
718-1000 829.0	63.8	17.7	3.55	1.81	0.92	5.85	2.47	0.62	0.04	0.03	< 0.01	0.02	1.86	98.6
Section B														
718-1260 715.0	37.7	3.39	15.2	31.9	1.89	< 0.05	0.05	0.2	0.02	0.14	0.57	0.01	9.78	100.8
718-1260 772.0	39.5	3.79	10.7	32.5	2.98	0.08	0.01	0.22	0.01	0.15	0.63	0.01	9.74	100.3
718-1260 824.0	38.4	3.62	12.1	31.8	2.46	< 0.05	0.05	0.19	0.02	0.14	0.55	0.01	9.83	99.1
718-1260 849.5	39	3.71	10.3	32.3	2.92	< 0.05	0.02	0.2	0.01	0.15	0.55	0.01	9.99	99.1
718-1260 901.5	38.6	3.04	11.7	35.4	3.11	0.09	0.14	0.17	0.02	0.16	0.69	0.01	7.41	100.6
718-1260 940.0	39.3	2.41	12.7	38.2	2.2	0.13	0.1	0.14	< 0.01	0.16	0.74	0.01	4.28	100.4
718-1260 963.0	39.1	2.25	14.3	39	2.26	0.1	0.15	0.13	< 0.01	0.17	0.73	0.01	2.35	100.5
718-1260 982.5	39.3	2.27	14.4	39.5	2.07	0.07	0.16	0.13	0.01	0.16	0.76	0.01	1.91	100.7
718-1260 1002.5	38.1	2.4	15.6	37.1	2.85	0.1	0.14	0.13	0.01	0.18	0.76	0.01	1.86	99.2
718-1260 1024.0	40.2	2.44	12.6	39.8	2.19	0.15	0.14	0.13	0.01	0.18	0.8	< 0.01	2.39	101.1
718-1260 1047.5	39.8	2.64	12.4	38.7	2.09	0.1	0.21	0.13	< 0.01	0.17	0.75	< 0.01	4.46	101.5
Section C														
718-1007 404.5	37.6	2.38	13.1	36.3	1.81	< 0.05	0.04	0.15	0.01	0.17	0.64	0.01	7.8	100
718-1007 484.0	37.4	2.44	11.1	37.9	1.42	0.07	0.04	0.13	< 0.01	0.15	0.73	0.01	7.2	98.6
718-1007 509.0	37.2	2.09	12.7	37.8	2.04	< 0.05	0.03	0.11	0.01	0.16	0.73	< 0.01	5.98	98.9

Sample ID	SiO2 %	Al2O3 %	Fe2O3 %	MgO %	CaO %	Na2O %	K2O %	TiO2 %	P2O5 %	MnO %	Cr2O3 %	V2O5 %	LOI %	Sum %
718-1007 545.5	38.4	2.05	11.6	39	2.31	0.11	0.05	0.11	0.01	0.16	0.71	0.01	4.51	99.1
718-1007 561.0	37.9	1.65	12	39.9	1.85	< 0.05	0.04	0.09	0.01	0.17	0.76	0.02	4.21	98.7
718-1007 563.0	38.4	1.86	11.8	40.1	2.18	0.1	0.03	0.1	< 0.01	0.16	0.74	0.01	4.12	99.5
718-1007 572.5	38.6	1.82	12.4	39.4	2.03	< 0.05	0.03	0.1	< 0.01	0.17	0.73	0.01	4.02	99.3
718-1007 631.5	38.6	1.65	12.3	40.5	1.89	0.05	0.03	0.1	0.02	0.16	0.77	< 0.01	3.28	99.3
718-1007 650.0	39.7	1.43	12.6	42.3	2	< 0.05	0.03	0.08	< 0.01	0.19	0.82	0.01	2.25	101.4
718-1007 682.0	38.6	1.81	12.1	40.2	1.88	0.06	0.04	0.14	0.02	0.15	0.77	0.01	4.4	100.2
718-1007 707.0	39	1.8	12.5	41.5	1.53	< 0.05	0.02	0.09	< 0.01	0.18	0.79	0.01	3.6	100.9
Section D														
718-949 12.0	39.4	2.66	12.6	37.4	2.63	0.11	0.14	0.14	0.02	0.19	0.77	0.01	4.68	100.8
718-949 18.0	39.6	2.61	12.9	37.1	2.82	0.11	0.14	0.16	< 0.01	0.18	0.8	< 0.01	4.57	101
718-949 18.6	39.5	2.61	13.1	37.4	2.63	0.06	0.08	0.14	< 0.01	0.17	0.78	< 0.01	4.7	101.2
718-949 27.5	39.7	2.79	12.9	37.2	2.73	0.09	0.12	0.16	0.02	0.18	0.78	0.01	4.99	101.7
718-949 38.5	39.4	2.93	13	36.8	3.46	0.08	0.14	0.18	0.02	0.2	0.8	0.02	4.5	101.5
718-949 49.5	39.9	3.04	12.6	35.6	3.03	0.12	0.26	0.21	0.02	0.19	0.74	< 0.01	5.87	101.5
718-949 67.5	39.6	3.05	12	35.7	2.98	0.06	0.19	0.18	0.02	0.17	0.76	0.01	6.1	100.8
718-949 81.5	39.3	3.3	12.4	34.2	3.31	0.12	0.12	0.21	0.02	0.19	0.72	0.02	6.23	100.2
718-949 91.5	39.6	3.67	12.5	33.6	3.55	0.06	0.15	0.24	0.01	0.19	0.7	0.02	6.44	100.8
718-949 103.5	39.6	4.21	12.6	31.5	3.97	0.09	0.18	0.24	0.02	0.2	0.63	0.02	7.62	100.9
Section E														
909-09 4.5	40.8	4.88	13.5	30	4.63	0.29	0.27	0.29	0.03	0.22	0.47	0.02	5.65	101.1
909-09 15.0	40.2	5.03	13.4	29.6	4.75	0.32	0.35	0.29	0.02	0.2	0.46	0.02	5.57	100.3
909-09 27.0	41.1	5.18	12.5	29	5.41	0.33	0.2	0.3	0.02	0.22	0.44	0.02	6.48	101.2
909-09 42.5	40.5	5.29	13.1	28.3	5.02	0.26	0.18	0.32	0.03	0.2	0.4	0.02	6.81	100.4
909-09 70.0	40.8	5.83	12.4	26.6	5.38	0.28	0.11	0.38	0.03	0.18	0.36	0.03	7.55	99.8
909-09 82.5	42	7.63	12.6	20.2	9.25	0.23	0.14	0.52	0.04	0.2	0.24	0.03	7.08	100.1
Duplicates														
718-1000 602.0	38.1	2.65	12.1	35.3	1.22	0.05	0.05	0.15	0.01	0.15	0.67	< 0.01	10.2	100.6
909-09 27.0	40.9	5.17	12.4	29.2	5.32	0.31	0.2	0.3	0.02	0.24	0.44	0.02	6.57	101
718-1007 545.5	38.5	2.13	11.7	39.4	2.32	0.12	0.04	0.12	< 0.01	0.17	0.72	< 0.01	4.52	99.7
718-949 18.0	39.3	2.62	12.8	37.1	2.8	0.09	0.13	0.16	0.02	0.19	0.8	0.01	4.57	100.6

WHOLE ROCK TRACE ELEMENT XRF ANALYSES

Sample ID	Ba ppm	Sr ppm	Y ppm	Zr ppm	Ni ppm	Cu ppm	Co ppm	Au ppb	Pt ppb	Pd ppb	S %
Section A											
718-1000 602.0	< 10	< 5	< 5	9	2890	229	139	10	17	53	0.36
718-1000 604.0	< 10	< 5	< 5	8	4160	813	171	18	64	193	0.51
718-1000 625.0	< 10	< 5	< 5	8	1950	64	126	13	8	24	0.31
718-1000 648.0	23	< 5	< 5	20	2540	257	136	9	16	49	0.42
718-1000 673.0	< 10	< 5	< 5	10	2140	284	136	9	18	57	0.35
718-1000 683.5	32	8	< 5	16	1680	114	134	7	7	28	0.34
718-1000 701.0	20	6	< 5	7	2130	239	131	6	10	36	0.15
718-1000 720.0	< 10	< 5	< 5	6	2630	211	130	7	24	77	0.22
718-1000 743.0	43	24	< 5	7	3460	477	160	10	66	186	0.44
718-1000 754.0	31	11	< 5	8	3160	670	157	19	68	221	0.37
718-1000 765.5	37	13	< 5	12	2070	42	128	< 5	< 5	6	0.05
718-1000 781.0	40	24	< 5	17	2320	221	130	14	32	99	0.19
718-1000 795.0	15	8	< 5	23	1440	56	109	< 5	< 5	5	0.12
718-1000 809.5	14	< 5	< 5	14	5880	1070	183	10	144	423	1.11
718-1000 818.0	< 10	< 5	< 5	19	10100	369	225	124	313	943	2.31
718-1000 829.0	654	85	16	241	270	1464	17	< 5	< 5	6	0.22
Section B											
718-1260 715.0	< 10	< 5	< 5	13	2950	673	168	19	42	114	1.07
718-1260 772.0	< 10	< 5	< 5	15	2480	94	159	< 5	11	31	0.23
718-1260 824.0	< 10	< 5	< 5	14	2920	485	155	< 5	49	137	0.98
718-1260 849.5	< 10	< 5	< 5	12	3920	750	195	14	46	160	1.57
718-1260 901.5	26	8	< 5	11	1790	87	127	< 5	< 5	12	0.31
718-1260 940.0	< 10	6	< 5	< 5	3570	369	153	< 5	36	98	0.47
718-1260 963.0	23	11	< 5	8	3810	567	204	25	68	159	1.08
718-1260 982.5	12	11	< 5	6	4080	501	202	24	56	133	1.08
718-1260 1002.5	19	11	< 5	8	5250	1163	225	34	89	151	1.94
718-1260 1024.0	29	12	< 5	9	2620	118	152	12	25	55	0.14
718-1260 1047.5	22	11	< 5	6	2360	57	147	< 5	8	33	0.1
Section C											
718-1007 404.5	< 10	< 5	< 5	10	2770	215	136	19	39	98	0.28
718-1007 484.0	< 10	< 5	< 5	9	2030	30	127	7	6	15	0.04
718-1007 509.0	< 10	< 5	< 5	6	4790	906	176	20	70	181	0.81
718-1007 545.5	< 10	< 5	< 5	8	2200	145	134	8	42	45	0.14
718-1007 561.0	< 10	< 5	< 5	< 5	3810	121	167	21	72	213	0.47

Sample ID	Ba ppm	Sr ppm	Y ppm	Zr ppm	Ni ppm	Cu ppm	Co ppm	Au ppb	Pt ppb	Pd ppb	S %
718-1007 563.0	12	< 5	< 5	6	2570	237	141	6	21	68	0.14
718-1007 572.5	13	< 5	< 5	< 5	3460	675	164	15	57	187	0.41
718-1007 631.5	< 10	< 5	< 5	< 5	3380	706	156	17	58	155	0.28
718-1007 650.0	< 10	< 5	< 5	7	3030	283	156	10	23	80	0.14
718-1007 682.0	< 10	< 5	< 5	10	3720	433	155	12	54	165	0.3
718-1007 707.0	< 10	< 5	< 5	< 5	2630	204	151	11	27	82	0.1
Section D											
718-949 12.0	13	16	< 5	11	1780	19	141	< 5	< 5	< 5	0.05
718-949 18.0	19	18	< 5	11	1720	17	135	5	< 5	9	0.03
718-949 18.6	< 10	21	< 5	9	1600	28	128	< 5	< 5	< 5	0.04
718-949 27.5	19	16	< 5	12	1610	15	125	< 5	< 5	< 5	0.03
718-949 38.5	20	19	< 5	12	1530	20	126	< 5	< 5	< 5	0.04
718-949 49.5	28	20	< 5	16	1470	12	120	< 5	< 5	< 5	0.03
718-949 67.5	23	13	< 5	12	1690	18	129	< 5	8	7	0.01
718-949 81.5	19	23	< 5	14	1640	45	118	< 5	< 5	< 5	0.03
718-949 91.5	33	24	< 5	14	1620	62	118	< 5	< 5	< 5	0.03
718-949 103.5	18	33	< 5	15	1380	61	113	< 5	< 5	< 5	0.01
Section E											
909-09 4.5	11	47	< 5	21	1290	91	112	< 5	< 5	< 5	0.01
909-09 15.0	37	42	6	18	1310	112	114	< 5	9	12	0.02
909-09 27.0	31	39	< 5	18	1270	13	109	< 5	< 5	6	0.01
909-09 42.5	21	22	6	20	1200	70	109	< 5	< 5	8	0.01
909-09 70.0	< 10	14	6	22	1070	12	104	5	< 5	8	0.01
909-09 82.5	< 10	62	10	26	600	30	71	< 5	< 5	< 5	< 0.01
Duplicates											
718-1000 602.0	< 10	< 5	< 5	10	2860	227	132	7	12	48	0.36
909-09 27.0	27	40	7	17	1240	12	107	< 5	< 5	6	0.02
718-1007 545.5	< 10	< 5	< 5	6	2270	145	134	13	31	57	0.09
718-949 18.0	< 10	21	< 5	9	1690	17	132	6	< 5	8	0.02

OLIVINE ELECTRON MICROPROBE MAJOR ELEMENT ANALYSES

Sample ID	SiO2	Al2O3	FeO	MgO	CaO	TiO2	MnO	Cr2O3	Total	Ni
	%	%	%	%	%	%	%	%	%	ppm
Section A										
718-1000 625.0	39.02	0.05	11.67	47.26	0.27	0	0.17	0.05	98.5	1680
718-1000 648.0	39.34	0.05	11.93	47.71	0.26	0.01	0.18	0.05	99.53	1573
718-1000 673.0	39.47	0.04	11.85	47.38	0.25	0.01	0.17	0.04	99.21	1474
718-1000 683.5	39.92	0.04	11.68	47.34	0.21	0	0.17	0.04	99.42	1170
718-1000 701.0	39.81	0.04	11.79	47.11	0.28	0	0.17	0.06	99.26	1920
718-1000 720.0	39.83	0.05	11.63	47.31	0.26	0.01	0.18	0.05	99.32	1996
718-1000 726.0	39.64	0.05	12.95	46.83	0.16	0.01	0.19	0.02	99.87	2331
718-1000 743.0	39.41	0.04	12.46	47.38	0.21	0.01	0.19	0.03	99.73	2137
718-1000 754.0	39.39	0.04	12.33	47.36	0.2	0.01	0.18	0.04	99.55	2190
718-1000 765.5	39.77	0.04	12.26	46.88	0.2	0.01	0.18	0.03	99.38	2380
718-1000 768.0	40.07	0.05	12.68	47.06	0.18	0.01	0.19	0.03	100.26	2547
718-1000 781.0	39.6	0.04	13.64	45.87	0.17	0.01	0.2	0.02	99.55	2207
718-1000 784.0	39.81	0.04	13.21	46.65	0.24	0.01	0.21	0.06	100.24	1120
718-1000 795.0	38.83	0.03	14.34	45.87	0.14	0.01	0.21	0.02	99.46	2010
Section B										
718-1260 901.0	39.21	0.05	12.35	47.11	0.22	0.01	0.18	0.04	99.18	1552
718-1260 940.0	38.98	0.05	12.35	47.39	0.25	0	0.18	0.04	99.24	1717
718-1260 963.0	39.3	0.04	12.23	47.43	0.24	0.01	0.18	0.04	99.47	1338
718-1260 982.0	39.15	0.06	12.08	47.46	0.25	0	0.18	0.04	99.22	1528
718-1260 1002.0	39.34	0.03	12.73	46.98	0.22	0.01	0.19	0.03	99.52	1551
718-1260 1024.0	39.28	0.05	12.18	47.36	0.2	0.01	0.18	0.03	99.29	1978
718-1260 1047.0	39.34	0.04	12.43	47.48	0.14	0.01	0.18	0.03	99.66	2442
Section C										
718-1007 404.5	39.39	0.05	14.38	45.25	0.24	0.01	0.19	0.04	99.56	2186
718-1007 484.0	39.62	0.05	12.05	47.08	0.22	0.01	0.18	0.05	99.24	2270
718-1007 509.0	39.62	0.05	12.29	47.01	0.18	0	0.18	0.03	99.36	2128
718-1007 545.5	39.86	0.04	12.08	47.33	0.18	0.01	0.18	0.04	99.71	2092
718-1007 563.0	39.77	0.04	11.87	47.24	0.15	0.01	0.17	0.04	99.3	2134
718-1007 572.5	39.68	0.05	11.89	47.16	0.18	0.01	0.17	0.03	99.17	2049
718-1007 604.0	39.68	0.04	11.95	47.1	0.2	0.01	0.18	0.03	99.18	2307
718-1007 631.5	39.92	0.04	11.61	47.48	0.18	0.01	0.17	0.03	99.43	2251
718-1007 650.0	39.96	0.04	11.63	47.43	0.18	0.01	0.17	0.03	99.45	2432
718-1007 682.0	39.77	0.03	11.82	47.31	0.17	0.01	0.17	0.03	99.31	2439
718-1007 707.0	39.9	0.03	11.86	47.24	0.16	0.01	0.18	0.03	99.41	2434

Sample ID	SiO2	Al2O3	FeO	MgO	CaO	TiO2	MnO	Cr2O3	Total	Ni
	%	%	%	%	%	%	%	%	%	ppm
Section D										
718-949 12.0	39.45	0.03	12.9	46.15	0.2	0.01	0.19	0.03	98.96	1996
718-949 18.0	39.36	0.03	13.23	45.93	0.2	0.01	0.2	0.02	98.99	1908
718-949 27.5	39.28	0.04	13.33	45.93	0.2	0.01	0.2	0.03	99.01	1964
718-949 38.5	39.17	0.04	13.51	45.97	0.18	0.01	0.19	0.03	99.1	1830
718-949 49.5	39.39	0.04	13.74	45.87	0.16	0.01	0.21	0.02	99.44	1833
718-949 67.5	39.6	0.03	13.21	46.2	0.15	0.01	0.19	0.02	99.41	2103
718-949 81.5	39.36	0.03	13.56	46.03	0.13	0.01	0.2	0.03	99.36	2228
718-949 91.5	39.36	0.03	14.14	45.77	0.16	0.02	0.21	0.02	99.71	2167
718-949 103.5	39.24	0.04	14.79	44.99	0.14	0.01	0.22	0.02	99.45	2013
Section E										
909-09 4.0	38.96	0.03	16.53	43.73	0.17	0.01	0.24	0.02	99.68	2019
909-09 15.0	38.94	0.03	16.45	43.8	0.2	0.01	0.24	0.02	99.69	1983
909-09 42.0	38.87	0.03	16.47	43.7	0.21	0	0.24	0.02	99.54	1967